Pharmacological Research 230 (2026) 108321

Contents lists available at ScienceDirect

Brazilian Journal of Health and Clinical Approaches

journal homepage: www.elsevier.com/bjhca

Tirzepatide, a dual GIP/GLP-1 receptor agonist, attenuates endothelial dysfunction and angiotensin II-induced abdominal aortic aneurysm in ApoE$^{-/-}$ mice

Álvaro Gómez-Martín [a,b], Patrice Marques [a,c,d], Cristina Arce-Recatalá [a,b], Ángela Vea [a,b], Elena Domingo [a,b], Blanca Alabadi [e,f], José T. Real [e,f,*], María-Jesús Sanz [a,b,f,**], Laura Piqueras [a,b,f,***]

[a] Department of Pharmacology, University of Valencia, Valencia, Spain
[b] Institute of Health Research-INCLIVA, Valencia, Spain
[c] Health Research Institute Hospital La Fe (IIS La Fe), Valencia, Spain
[d] CIBEREHD-Spanish Biomedical Research Center in Hepatic and Digestive Diseases, Carlos III Health Institute (ISCIII), Madrid, Spain
[e] Endocrinology and Nutrition Service, University Clinic Hospital of Valencia, Valencia, Spain
[f] CIBERDEM-Spanish Biomedical Research Center in Diabetes and Associated Metabolic Disorders, Carlos III Health Institute (ISCIII), Madrid, Spain

ARTICLE INFO

Keywords:
Abdominal aortic aneurysm
GLP-1 receptor
GIP receptor
Angiotensin-II
Inflammation
Endothelial dysfunction, tirzepatide

ABSTRACT

Endothelial dysfunction is a critical initiating event in abdominal aortic aneurysm (AAA), a condition posing a high risk of a fatal rupture. Dual glucagon-like peptide-1 (GLP-1) and glucose-dependent insulinotropic peptide (GIP) receptor agonists have emerged as potent treatments for diabetes and obesity, with clinical evidence suggesting broader cardiovascular benefits. However, the direct impact of tirzepatide (dual GLP-1R/GIPR agonist) on endothelial dysfunction and AAA pathogenesis remains poorly understood. We investigated the effects of dual GLP-1R/GIPR agonism on endothelial dysfunction and AAA development.

We employed parallel-plate flow chamber assays to evaluate the effects of tirzepatide on TNFα-induced leukocyte–endothelium interactions. Expression of GLP-1R, GIPR, adhesion molecules (VCAM-1 and ICAM-1), and NF-κB activation was quantified using immunofluorescence and western blotting. The *in vivo* efficacy of tirzepatide was assessed using an angiotensin-II-infused *apoE*$^{-/-}$ mouse model of AAA.

GLP-1R and GIPR were expressed in human endothelial cells and murine suprarenal aortas. Tirzepatide significantly attenuated TNFα-induced leukocyte–endothelium interactions, downregulated VCAM-1/ICAM-1/CX_3CL1 expression, and inhibited the mRNA expression and generation of MCP-1 and RANTES. Mechanistically, these effects were driven by the suppression of NF-κB activation. Chronic subcutaneous administration of tirzepatide over 28 days significantly limited suprarenal aortic expansion and reduced AAA incidence in Ang-II-infused mice. This vasoprotective effect was characterized by preserved elastin integrity, reduced neovessel formation, and diminished macrophage accumulation within the aneurysmal wall.

Dual GLP-1R/GIPR agonism mitigates endothelial dysfunction and suppresses inflammatory pathways driving AAA progression. These findings position tirzepatide as a promising therapeutic strategy for the prevention of vascular remodeling and AAA development.

1. Background

Abdominal aortic aneurysm (AAA) is a chronic vascular pathology defined by the localized dilation of the abdominal aorta, posing a substantial risk of life-threatening rupture [1]. This condition is highly prevalent among the elderly, affecting approximately 4–8% of men and

* Correspondence to: Endocrinology and Nutrition Service, University Clinic Hospital of Valencia, Avda. Blasco Ibáñez 17, Valencia 46010, Spain.
** Correspondence to: Department of Pharmacology, Faculty of Medicine, University of Valencia, Avda. Blasco Ibáñez 15, Valencia 46010, Spain.
*** Correspondence to: Department of Pharmacology, Faculty of Pharmacy and Food Sciences, University of Valencia, Avda. Vicente Andrés Estelles, s/n, Burjassot 46100, Spain.
E-mail addresses: jose.t.real@uv.es (J.T. Real), maria.j.sanz@uv.es (M.-J. Sanz), laura.piqueras@uv.es (L. Piqueras).

https://doi.org/10.1016/j.phrs.2026.108321
Received 13 February 2026; Received in revised form 19 June 2026; Accepted 23 June 2026
Available online 24 June 2026

2% of women over the age of 65. Primary risk factors for AAA include male sex, advanced age, smoking, genetic predisposition, hypercholesterolemia, and hypertension [2]. Additionally, several studies have demonstrated an association between sympathomimetic recreational drugs such as cocaine and acute aortic rupture [3]. Currently, there is no effective pharmacotherapy to halt AAA progression, and clinical management is mainly restricted to surgical intervention [4]. Given the high morbidity and mortality associated with aortic rupture, there is a critical need to identify novel pharmacological targets capable of attenuating aneurysm expansion and improving patient outcomes.

Endothelial dysfunction and chronic inflammation are fundamental drivers of the progressive remodeling and structural weakening of the vessel wall in AAA [5,6]. Central to this process is macrophage accumulation, which plays a pivotal role in AAA pathophysiology by secreting pro-inflammatory chemokines/cytokines and matrix metalloproteases (MMPs) that facilitate aortic structural disruption [7]. This inflammatory cascade is often mediated by angiotensin-II (Ang-II), the primary effector peptide of the renin-angiotensin system, which is heavily implicated in both vascular inflammation and pathological expansion [8,9]. Consequently, the 28-day infusion of Ang-II in hypercholesterolemic mice has become a gold-standard preclinical model for studying AAA [10,11]. This model effectively recapitulates the hallmark pathological features of human AAA, including robust chemokine and MMP release, leukocyte infiltration, degradation of the aortic elastic laminae, and enhanced neovessel formation [8].

Tirzepatide, a dual glucagon-like peptide−1 (GLP−1) and glucose-dependent insulinotropic peptide (GIP) receptor agonist, has recently been approved for the treatment of type 2 diabetes (T2D) and obesity, demonstrating superior efficacy in improving glycemic control and reducing body weight compared with selective GLP−1R agonists [12–14]. Beyond metabolic regulation, tirzepatide has shown therapeutic promise in metabolic dysfunction-associated steatotic liver disease and other systemic metabolic conditions [15]. Clinical evidence further suggests significant cardiovascular benefits, as tirzepatide is associated with the reduction of key risk factors, including hypertension, dyslipidemia, and chronic systemic inflammation [16,17]. Moreover, dual GLP−1R/GIPR agonism has been linked to improved cardiac function, metabolic control, and functional capacity in patients with heart failure [18].

Despite these multi-organ benefits, the specific impact of dual GLP−1R/GIPR agonism on endothelial dysfunction and the pathogenesis of AAA remains largely unexplored. In the present study, we sought to evaluate the impact of dual GLP−1R/GIPR agonism on vascular dysfunction and AAA growth using both *in vitro* and *in vivo* approaches.

2. Methods

2.1. In vitro studies

2.1.1. Cell culture

All research with human samples complied with the principles outlined in the Declaration of Helsinki and also those approved (N°. 2021/047) by the Institutional Ethics Committee of the University Clinic Hospital of Valencia (Valencia, Spain). Written informed consent was obtained from all volunteers.

Human umbilical vein endothelial cells (HUVEC) were isolated by collagenase treatment [19] and maintained up to passage 2 in human endothelial cell-specific medium (EBM−2, Lonza, Basel, Switzerland) supplemented with endothelial growth media (EGM−2, Lonza) and 10% fetal bovine serum (FBS, Biowest, Nuaille, France). Before every experiment, HUVEC were incubated for 24 h in medium containing 1% FBS.

2.1.2. Quantification of soluble chemokines in cell supernatants

HUVEC were grown to confluence and stimulated with tumor necrosis factor-α (TNFα, 20 ng/mL; Thermo Fisher Scientific, Waltham, MA) for 24 h. To assess the effects of dual receptor agonism, specific plates were preincubated with tirzepatide (1–100 nM, MedChemExpress, Monmouth Junction, NJ) for 24 h prior to TNFα stimulation. The release of human monocyte chemoattractant protein−1 (MCP−1)/CCL2 and regulated on activation normal T-cell expressed and secreted (RANTES/CCL5) was quantified in HUVEC supernatants using commercial enzyme-linked immunosorbent assay (ELISA) kits (DuoSet; R&D Systems, Abingdon, UK).

2.1.3. Leukocyte–HUVEC interactions under flow conditions

To evaluate leukocyte–endothelial cell interactions under dynamic conditions, a parallel-plate flow chamber assay was performed as previously described [20]. HUVEC were grown to confluence and preincubated with tirzepatide (100 nM; MedChemExpress, Monmouth Junction, NJ) for 24 h. After this pretreatment period, the culture medium was replaced and cells were stimulated with TNFα (20 ng/mL; Thermo Fisher Scientific, Waltham, MA) or an additional 24 h in the presence of freshly added tirzepatide. To determine the receptor-specific contributions, a selective GLP−1R antagonist (exendin(9-39), 1 μM) and/or a selective GIPR antagonist (GIP(3-30), 1 μM) were added (both from MedChemExpress, Monmouth Junction, NJ) 1 h before tirzepatide treatment. The flow chamber (GlycoTech, Gaithersburg, MD) was assembled and mounted on an inverted phase-contrast microscope (Axio Observer A1, ZEISS, Oberkochen, Germany). Whole blood from healthy donors (diluted 1:10 in Hank's balanced salts solution) was perfused across HUVEC monolayers at a shear stress of 0.5 dyn/cm^2 [21,22]. Stable leukocyte adhesion was quantified after 5 min of perfusion. For each experimental condition, at least five independent fields were recorded (×20 objective, ×10 eyepiece) for 10 s, as described [23]. The resulting images were digitized and analyzed to determine the average number of adherent cells per field.

2.1.4. Western blotting

Following the experimental treatments, HUVEC were washed with phosphate-buffered saline (PBS) and lysed using RIPA buffer supplemented with protease and phosphatase inhibitors (Pierce™ RIPA Buffer and Halt Protease and Phosphatase Inhibitor Single-Use Cocktail 100 ×, Thermo Fisher Scientific, Waltham, MA). Cells were incubated on ice with gentle agitation for 15 min, subsequently scraped, and the resulting whole-cell lysates were transferred to a microcentrifuge tube and rotated for 30 min at 4°C to ensure complete cell lysis and protein extraction. The lysates were then centrifuged, and total protein concentration was determined *via* the bicinchoninic acid (BCA) assay using the Pierce™ BCA Protein Assay Kit (Thermo Fisher Scientific).

Protein samples were denatured in loading buffer containing β-mercaptoethanol at 95ºC for 5 min. Equal amounts of protein were subjected to sodium dodecyl sulphate polyacrylamide gel electrophoresis using a 12% acrylamide running gel and subsequently transferred onto polyvinylidene difluoride (PVDF) membranes (Amersham Hybond 0.2 μm PVDF blotting membrane, GE Healthcare, Chicago, IL). Non-specific binding sites were blocked with 2% BSA in Tris-buffered saline (TBS) containing 0.1% Tween−20 solution for 1 h. The membranes were then incubated overnight with the appropriate primary antibody: rabbit IgG polyclonal antibody against human GIPR (#Cat: ab136266, #Lot: 1048958–6, dilution 1:200, Abcam, Cambridge, UK), mouse IgG_{2a} monoclonal antibody against human GLP−1R (#Cat: sc390774, #Lot: L1321, dilution 1:2000, Santa Cruz Biotechnology, Dallas, TX), rabbit IgG monoclonal antibody against human nuclear factor-kappa B (NF-κB)/p65 (#Cat: 8242, #Lot: 20, dilution 1:500, Cell Signaling Technology, Danvers, MA), rabbit IgG polyclonal antibody against human phosphorylated-NF-κB/p65 (#Cat: 3031, #Lot: 14, dilution 1:300, Cell Signaling Technology), rabbit IgG monoclonal antibody against human c-Jun (#Cat: ab40766, #Lot: 1058316–47, dilution 1:500, Abcam), rabbit IgG monoclonal antibody against human phosphorylated-c-Jun (#Cat: ab32385, #Lot: 1121314–2, dilution 1:500, Abcam), and mouse IgG_{2b} monoclonal antibody against human β-actin (#Cat: 3700,

#Lot: 18, dilution 1:2000, Cell Signaling Technology). Membranes were subsequently washed, incubated for an additional hour with the secondary horseradish peroxidase (HRP)-conjugated anti-rabbit antibody (#Cat: P0448, #Lot: 41424306, 1:2000 dilution) or HRP-conjugated anti-mouse antibody (#Cat: P0447, #Lot: 41456532, 1:2000 dilution; both from Dako-Agilent Technologies, Santa Clara, CA) and developed using the Amersham ECL Western Blotting Reagent (GE Healthcare). Signals were recorded using a luminescent analyzer (FujiFilm Image Reader LAS 4000, Fuji, Tokyo, Japan) and analyzed with ImageJ software (Windows free version, developed by NIH, Bethesda, MD).

2.1.5. Immunofluorescence

HUVEC were grown to confluence on glass coverslips. Following the experimental treatments, HUVEC were washed twice with ice-cold PBS, fixed with 4% paraformaldehyde, and blocked in a TBS solution with 1% BSA. For protein localization, HUVEC were incubated at 4ºC overnight with the following primary rabbit antibodies against human: GLP−1R (IgG polyclonal, #Cat: sc390774, #Lot: L1321, dilution 1:100, Santa Cruz Biotechnology, Dallas, TX), GIPR (IgG polyclonal, #Cat: ab136266, #Lot: 1048958–6, dilution 1:500, Abcam, Cambridge, UK), VCAM−1 (IgG polyclonal, #Cat: 500-P300, #Lot: 1011M490RB J0418, dilution 1:50, Thermo Fisher Scientific, Waltham, MA), ICAM−1 (IgG polyclonal, #Cat: 500-P287, #Lot: 0909M464Rb J2609, dilution 1:100, Thermo Fisher Scientific), CX_3CL1/fractalkine (IgG polyclonal, #Cat: ab25088, #Lot: GR18924–35, dilution 1:200, Abcam), or NFκB (IgG monoclonal, #Cat: ab76311, #Lot: GR149932–8, dilution 1:100, Abcam). Primary antibodies were diluted in a 0.1% BSA/TBS solution. Immunofluorescence signals were visualized using Alexa Fluor 488-conjugated goat anti-rabbit (1:1000 dilution, #Cat: A−11034, #Lot: 2256692) or Alexa Fluor 488-conjugated goat anti-mouse (1:1000 dilution, #Cat: A−11001, #Lot: 1752514; both from Molecular Probes, Carlsbad, CA) secondary antibodies, incubated for 1 h at room temperature. Cell nuclei were counterstained with Hoechst dye (1:4000 dilution, Sigma-Aldrich, St. Louis, MO) for 20 min at room temperature. Images were captured with a fluorescence microscope (Axio Observer A1, ZEISS, Oberkochen, Germany) equipped with a 63 × objective lens and a 10 × eyepiece.

2.2. In vivo studies

All animal procedures and experiments adhered to ethical regulations and were approved by the Ethics Review Committee of the School of Medicine, University of Valencia and the Valencian regional authorities (ref. VSC187–186 PEA−0260). All animal experiments complied with the ARRIVE (Animal Research: Reporting of In Vivo Experiments) guidelines. These procedures complied with the EU Directive 2010/63/EU for the protection of animals used for scientific purposes and the EU Commission Recommendation 2007/526/EC on guidelines for the accommodation and care of animals used for experimental and other scientific purposes, as implemented in Spanish law under *Real Decreto* 1201/2005. All efforts were made to minimize the number of animals used and their suffering. Apolipoprotein E knockout (*apoE*$^{-/-}$) C57BL/6 male mice were supplied by Charles River Laboratories (Chatillon-sur-Chalaronne, France). Mice were housed under specific pathogen-free conditions with *ad libitum* access to a standard chow diet and water. Environmental conditions were maintained at a constant temperature of 22 ± 2°C and 60–65% humidity, following a 12-h light/dark cycle (lights on at 08:00 h).

2.2.1. Experimental protocol of aortic aneurysm induced by Ang-II

To induce AAA formation, 10-week-old male apoE-/- C57BL/6 mice were implanted with osmotic minipumps (Alzet, Model 2004, Charles River Laboratories, Chatillon-sur-Chalaronne, France). Under anesthesia (1.5–2% isoflurane) and maintained on a heating blanket, a small dorsal incision was made in the neck for the subcutaneous (sc) placement of the pumps. These pumps delivered either angiotensin-II (Ang-II; Calbiochem, San Diego, CA) at a rate of 1.44 mg/kg/day or sterile saline (0.9% NaCl) as a control for 28 days [10]. Following implantation, the incisions were sutured and the surgical site was disinfected. Tirzepatide or vehicle treatments were initiated on the same day as Ang-II infusion and maintained throughout the 28-day experimental period. Ang-II infused apoE$^{-/-}$ C57BL/6 mice were randomly allocated into four experimental groups: i) control saline-infused (n = 12, sc); ii) treatment with vehicle (n = 12, sc); iii) treatment with tirzepatide at a dose of 10 nmol/kg/day (n = 12, sc), and iv) treatment with tirzepatide at a dose of 30 nmol/kg/day (n = 12, sc). The selected doses of tirzepatide were based on established efficacy and pharmacokinetic profiles in murine models [24,25].

2.2.2. Measurement of blood pressure

Systolic blood pressure was monitored in conscious mice using a non-invasive tail-cuff system (CODA−6, Kent Scientific, Torrington, CT) according to previously established methods [26]. To ensure accurate readings and peripheral vasodilation, animals were placed in a restrainer on a warming chamber maintained at 37°C (Model LE5510, PANLAB, Barcelona, Spain). Mice underwent a one-week acclimatization period prior to baseline measurements and osmotic pump implantation. To account for circadian variations in vascular tone, all measurements were consistently recorded between 09:00 and 11:00 h.

2.2.3. Morphological analysis of AAA

On day 28, mice were deeply anesthetized with xylazine (1 mg/kg) and ketamine (150 mg/kg) *via* intraperitoneal injection. Unconscious animals were then euthanized by exsanguination *via* direct cardiac puncture, and 0.8 mL of blood was collected. Plasma was isolated by centrifugation and stored at −80ºC for subsequent analyses. Left cardiac ventricles were immediately perfused with PBS (10 mL) with an exit *via* the severed right atrium. The aorta was carefully exposed under a dissecting microscope, and periadvential tissue was removed. To determine the maximal outer diameter of the suprarenal aorta *ex vivo*, digital images were captured (Leica DMD108; Leica Microsystems, Wetzlar, Germany) and analyzed using ImageJ software (Windows free version, developed by NIH, Bethesda, MD). Aneurysm severity was classified (stage I to stage IV) by an investigator blinded to the experimental groups, based on a previous study [27]: stage I, dilated suprarenal lumen without thrombus or with minimal thrombus; stage II, pronounced bulbous suprarenal dilation in the suprarenal region containing a thrombus; stage III, multiple aneurysms; stage IV, ruptured aneurysm. Necropsies were performed on all mice that died during the 28-day treatment period. Aortic rupture was defined by the presence of blood clots within the retroperitoneal cavity (abdominal aortic rupture). While these animals were excluded from morphological tissue analysis due to post-mortem degradation, they were included in the final mortality and rupture rate calculations. Aneurysm characterization was performed on aortas harvested from surviving mice at the study endpoint or during the necropsy of mice that succumbed to aortic rupture [27].

2.2.4. Determination of biochemical parameters

Following a 12-hour fast [28], blood was collected by cardiac puncture under anesthesia, as described above. Plasma was isolated by centrifugation and stored at −80°C for further analysis. Total cholesterol, triglycerides, and high-density lipoprotein cholesterol (HDL-C) concentrations were determined using enzymatic colorimetric procedures (Wako Pure Chemicals Industries, Cape Charles, VA). Blood glucose levels were measured using the Contour® Next USB Blood glucose meter (Bayer HealthCare, Basel, Switzerland).

2.2.5. Histological and immunohistochemical analysis

Suprarenal aorta samples were fixed in 4% paraformaldehyde, embedded in paraffin, and sectioned at a thickness of 5 μm. Sections were mounted on Superfrost™ plus slides (J1800AMNZ; Thermo Fisher Scientific, Waltham, MA) for examination. General histological

morphology was assessed *via* hematoxylin and eosin (H&E) staining (Sigma-Aldrich, St. Louis, MO). Weigert Van Gieson staining (Bio-Optica, Milan, Italy) was performed to evaluate elastic fibers. Elastin degradation was qualitatively assessed under 40 × magnification by a blinded observer using digital images and a semiquantitative grading system, as described [29]. Elastin preservation was graded as follows: grade 1, non-elastin degradation, well-organized elastin laminae; grade 2, elastic laminae with occasional interruptions and breaks; grade 3, elastic laminae with multiple interruptions and breaks; grade 4, severe elastin fragmentation or loss.

Inflammatory infiltration and microvessel formation were also measured in aortic cross-sections. Endogenous peroxidase activity was quenched with 0.3% H_2O_2, followed by sequential blocking of endogenous biotin/streptavidin sites and non-specific binding using normal goat serum. Sections were incubated overnight at 4ºC with the following primary antibodies: i) smooth muscle cell (SMC) staining was carried out using a Cy3-conjugated goat IgG monoclonal antibody against mouse alpha smooth muscle actin (#Cat: C6198, #Lot: 037M4783V, dilution 1:100, Sigma-Aldrich); ii) CD31 staining was performed with a rabbit IgG polyclonal antibody against mouse CD31 (#Cat: ab28364, #Lot: 1109707–16, dilution 1:50, Abcam, Cambridge, UK); iii) for MMP analysis, we used a rabbit IgG polyclonal antibody against mouse MMP−2 (#Cat: ab37150, #Lot: GR286050–13, dilution 1:1000, Abcam) or against mouse MMP−9 (#Cat: sc−10737, #Lot: F1014, dilution 1:100, Santa Cruz Biotechnology, Dallas, TX); iv) for macrophage detection, we used a rat IgG_1 monoclonal antibody against mouse Mac3 (#Cat: sc−19991, #Lot: A3119, dilution 1:100, Santa Cruz Biotechnology).

Primary antibody labeling was detected suing either biotin-conjugated goat anti-rabbit (#Cat: 65–6140, #Lot: AA392265, dilution 1:200, Molecular Probes/Invitrogen, Carlsbad, CA) or biotin-conjugated goat anti-rat (#Cat: 31830, #Lot: AC4666481, dilution 1:200, Molecular Probes/Invitrogen) secondary antibody, followed by HRP-conjugated streptavidin (#Cat: SA−5704–100, #Lab: ZL0223, Vector Laboratories, Newark, CA). Signals were visualized using 3'-diaminobenzidine (DAB, SK−4100, Vector Laboratories) and sections were counterstained with Harris Hematoxylin (Sigma-Aldrich) and dehydrated. Fields from each suprarenal aortic section were captured (Axio Observer A1, ZEISS, Oberkochen, Germany), digitized, and analyzed (ImageJ, Windows free version, developed by NIH, Bethesda, MD).

2.2.6. Quantitative RT-PCR for mRNA expression

Total RNA was extracted from human endothelial cells and murine aortas using TRIzol RNA Reagent (Life Technologies, Thermo Fisher Scientific, Waltham, MA) and purified by standard methods. Reverse transcription was performed using 1 μg of total RNA and the TaqMan reverse transcription reagent kit (Applied Biosystem, Thermo Fisher Scientific). cDNA was amplified using a TaqMan Universal PCR Master Mix (Applied Biosystem, Thermo Fisher Scientific) and specific TaqMan probes (all pre-designed by Applied Biosystems) for human *MCP−1/CCL2* (Hs00234140_m1), *RANTES/CCL5* (Hs00174575_m1), *ICAM−1* (Hs00164932_m1), *VCAM−1* (Hs01003372_m1), *CX_3CL1* (Hs00171086_m1), and for mouse *Mcp−1/Ccl2* (Mm00441242_m1), *Rantes/Ccl5* (Mm01302427_m1), vascular endothelial growth factor (*Vegf*, Mm00437306_m1), *Gipr* (Mm01316344_m1) and *Glp−1r* (Mm00445292_m1) on a QuantStudio 5 Real-Time PCR (RT-PCR) System (Applied Biosystems, Thermo Fisher Scientific). Relative quantification of the different transcripts was determined by the $2^{-\Delta\Delta Ct}$ method using *Gapdh* (Mm99999915_g1, Applied Biosystem, Thermo Fisher Scientific) as an endogenous control [30].

2.3. Statistical analysis

Data are expressed as individual data points, percentages, or means ± standard error of the mean (SEM). To assess the statistical significance of aneurysm subtype variables, *chi-square* test was performed. Kaplan-Meier survival curves were constructed and analyzed using the log-rank (Mantel-Cox) test. One-way analysis of variance (ANOVA) followed by Tukey *post hoc* test was used for data that passed both normality and equal variance; otherwise, a non-parametric Kruskal-Wallis test followed by Dunn's *post hoc* analysis was used. Data were considered statistically significant at $p < 0.05$. The statistical analyses were conducted using GraphPad Prism software (version 8.0.2, GraphPad Software, Inc., La Jolla, CA).

3. Results

3.1. Tirzepatide reduces TNFα-induced endothelial chemokine release and leukocyte-endothelium interactions

We first confirmed the expression of both GLP−1R and GIPR in HUVEC. Western blot analyses demonstrated basal endothelial expression of both receptors (Fig. 1**A–C**), which remained unchanged following TNFα stimulation and/or tirzepatide treatment (Fig. 1**B–C**). Immunofluorescence analysis confirmed the localization of GLP−1R and GIPR on the endothelial cell membrane (Fig. 1**D**).

Because TNFα stimulation triggers endothelial production of CC chemokines, we evaluated whether tirzepatide modulates this response. ELISA analysis of HUVEC supernatants revealed that 24 h of TNFα stimulation significantly increased the secretion of MCP−1/CCL2 ($p < 0.0001$) and RANTES/CCL5 ($p < 0.0001$) (Fig. 1**E–F**). Notably, pretreatment with 100 mM tirzepatide significantly attenuated these increases for MCP−1/CCL2 ($p = 0.0103$, Fig. 1**E**) and RANTES/CCL5 ($p < 0.0001$, Fig. 1**F**). Consistent with these findings, RT–PCR analyses demonstrated that tirzepatide also reduced TNFα-induced *Mcp−1* and *Rantes* mRNA expression ($p = 0.013$ and $p = 0.015$ respectively, Figure I in the online-only Data Supplement, Fig. IA and B). Importantly, the simultaneous blockade of GLP−1R and GIPR completely abolished the inhibitory effect of tirzepatide ($p < 0.05$; Fig. IA-IB), indicating that activation of both receptors is required for its anti-inflammatory action.

To assess the functional implications of these findings, we performed dynamic flow chamber assays to evaluate leukocyte–endothelial cell interactions [20]. Diluted whole blood from healthy volunteers was perfused across HUVEC monolayers. As expected, TNFα stimulation significantly increased leukocyte adhesion compared with vehicle-treated cells ($p < 0.0001$; Fig. 1**G**). Remarkably, tirzepatide treatment significantly reduced TNFα-mediated leukocyte adhesion by 63.1% ($p < 0.0001$, Fig. 1**G**). This inhibitory effect was partially reversed by pretreatment with either the GLP−1R antagonist exendin (9–39) ($p = 0.024$) or the GIPR antagonist GIP (3–30) ($p = 0.029$, Fig. 1**G**). Furthermore, simultaneous blockade of both GLP−1R and GIPR completely abolished the suppressive effect of tirzepatide on leukocyte–endothelial cell interactions ($p < 0.0001$, Fig. 1**G**).

3.2. Tirzepatide attenuates TNFα-induced increased ICAM−1 and VCAM−1 expression in human endothelial cells

To determine if the inhibitory effects of tirzepatide on leukocyte adhesion were mediated by the modulation of endothelial cell adhesion molecule (CAM) expression, we measured the protein expression of intercellular adhesion molecule−1 (ICAM−1) and vascular cell adhesion molecule−1 (VCAM−1). Immunofluorescence analysis revealed that TNFα stimulation significantly upregulated both ICAM−1 ($p < 0.0001$) and VCAM−1 ($p < 0.0001$) expression when compared with unstimulated controls (Fig. 2**A–C**). Pretreatment of cells with tirzepatide significantly decreased TNFα-induced expression of ICAM−1 by 57.4% ($p < 0.0001$, Fig. 2**A–B**) and VCAM−1 by 48.5% ($p < 0.0001$, Fig. 2**A** and **C**). This inhibitory effect was partially reversed by cotreatment with either the GLP−1R antagonist exendin (9–39) or the GIPR antagonist GIP (3–30) for both ICAM−1 and VCAM−1 ($p < 0.0001$ for both, Fig. 2**B–C**). Notably, simultaneous blockade of both GLP−1R and GIPR

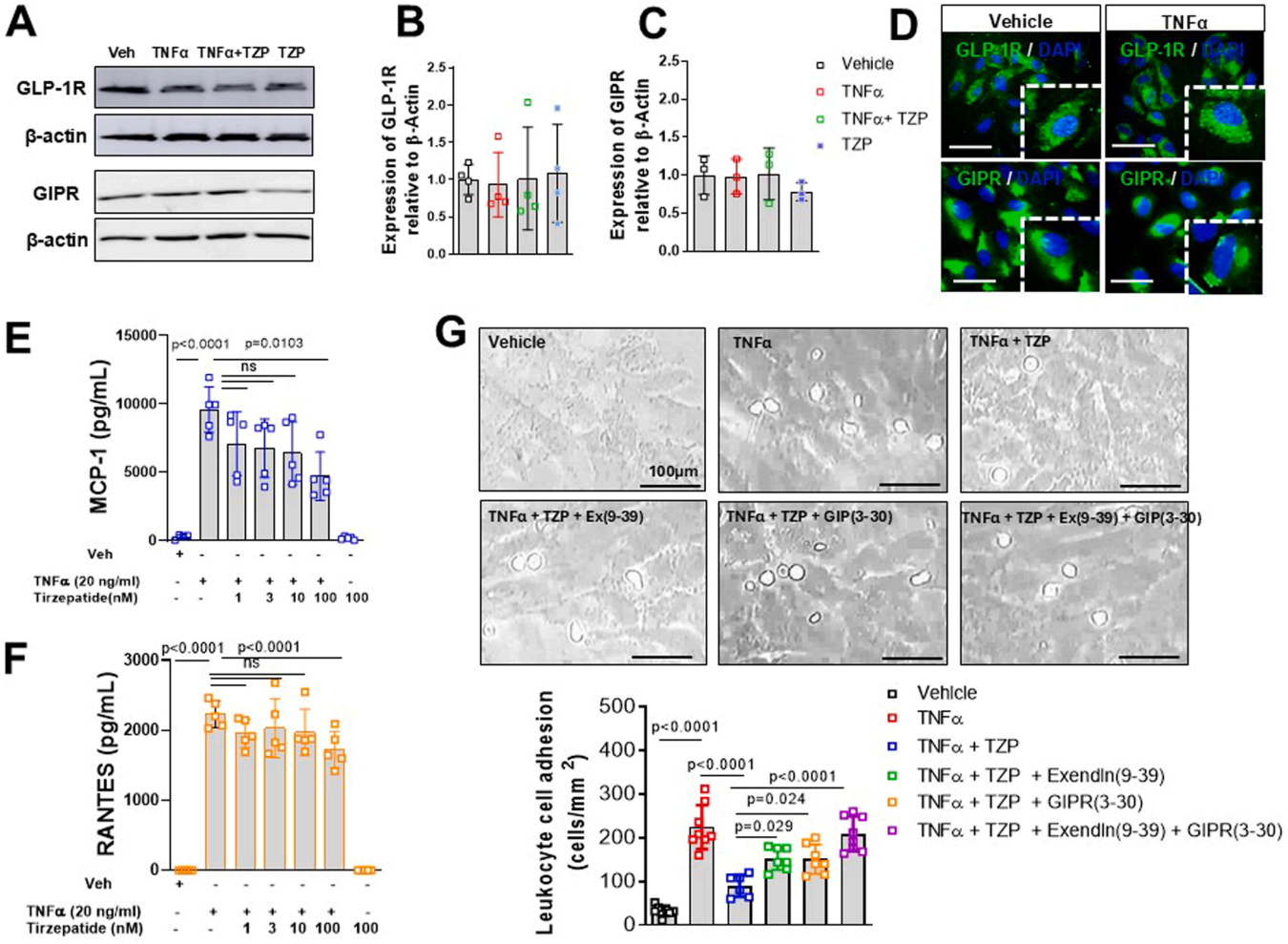

Fig. 1. Tirzepatide attenuates TNFα-induced endothelial pro-inflammatory chemokine release and leukocyte–endothelium interactions. A-C Representative western blot analysis of (A) GLP−1R and GIPR protein expression in HUVEC treated with vehicle, TNFα (20 ng/mL), TNFα + tirzepatide (TZP) (100 nM), or TZP alone (100 nM). Densitometric analysis is shown as protein expression ratios for (B) GLP−1R/β-actin (C) or GIPR/β-actin. Data represent the mean ± SEM of 3–4 independent experiments. Data were analyzed by one-way ANOVA followed by Tukey *post hoc* test. **D** Representative immunofluorescence analysis of GLP−1R and GIPR expression (*green*) in HUVEC. Nuclei are counterstained with DAPI (*blue*). Scale bar = 20 µm. **E–F** Pro-inflammatory chemokine secretion. Concentrations of (E) MCP−1/CCL2 and (F) RANTES/CCL5 (pg/mL) in HUVEC supernatants measured by ELISA. Data represent the mean ± SEM of 5 independent experiments. Data were analyzed by one-way ANOVA followed by Tukey *post hoc* test. **G** Leukocyte–endothelial interactions. Diluted blood (1:10 in HBSS) from healthy donors was perfused across endothelial monolayers for 5 min at 0.5 dyn/cm^2 (scale bar = 100 µm) and leukocyte adhesion was quantified as cells/mm^2. HUVEC were preincubated with TZP (100 nM) 24 h before stimulation with TNFα (20 ng/mL) for 24 h. In some plates, exendin (9–39) (GLP−1R antagonist; 1 µM) and/or GIP (3−30) (GIPR antagonist; 1 µM) were added 1 h before TZP treatment. Representative images of leukocyte-endothelial cell interactions are shown. Data represent the mean ± SEM of 4–8 independent experiments. Data were analyzed by one-way ANOVA followed by Tukey *post hoc* test.

markedly abrogated the suppressive effect of tirzepatide on TNFα-induced ICAM−1 and VCAM−1 expression ($p < 0.0001$, Fig. 2**A–C**). Consistent with these protein data, RT–PCR analysis demonstrated that tirzepatide significantly reduced TNFα-induced *Icam−1* and *Vcam−1* mRNA expression ($p = 0.004$ and $p = 0.007$ respectively, Figure I in the online-only Data Supplement, Fig. IC and D). Importantly, combined blockade of GLP−1R and GIPR completely abolished the inhibitory effect of tirzepatide ($p < 0.05$; Figure I in the online-only Data Supplement, Fig. IC and D).

These findings prompted us to further investigate the effect of tirzepatide on the expression of the membrane-bound chemokine fractalkine/CX_3CL1. Immunohistochemical analysis revealed that TNFα markedly induced fractalkine/CX_3CL1 expression in HUVECs ($p < 0.0001$ Fig. 3**A–B**), whereas pretreatment with tirzepatide significantly attenuated this response ($p < 0.0001$). Of note, simultaneous blockade of GLP−1R and GIPR prevented the inhibitory effect of tirzepatide, indicating that dual receptor activation is required for the suppression of TNFα-induced fractalkine/CX_3CL1 expression ($p < 0.0001$, Fig. 3**B**). Consistent with these findings, RT–PCR analysis demonstrated that tirzepatide significantly reduced TNFα-induced *Cx3cl1* mRNA expression. Furthermore, simultaneous blockade of GLP−1R and GIPR prevented this inhibitory effect ($p = 0.037$, Fig. 3**C**), further supporting the requirement of dual receptor activation for the anti-inflammatory actions of tirzepatide.

3.3. *Tirzepatide inhibits TNFα-induced NF-κB/p65 signaling in human endothelial cells*

The NF-κB signaling cascade is a central mediator of TNFα-induced CAM expression and chemokine release [31]. Accordingly, we investigated the impact of tirzepatide on NF-κB pathway activation. Immunofluorescence analysis showed that a 30-min stimulation with TNFα induced significant translocation of the NF-κB/p65 subunit into the nucleus ($p < 0.0001$, Fig. 4**A–B**). Notably, tirzepatide pretreatment reduced this TNFα-induced nuclear translocation by 88.5% ($p < 0.0001$, Fig. 4**A–B**). While cotreatment with either exendin (9–39) or GIP (3–30)

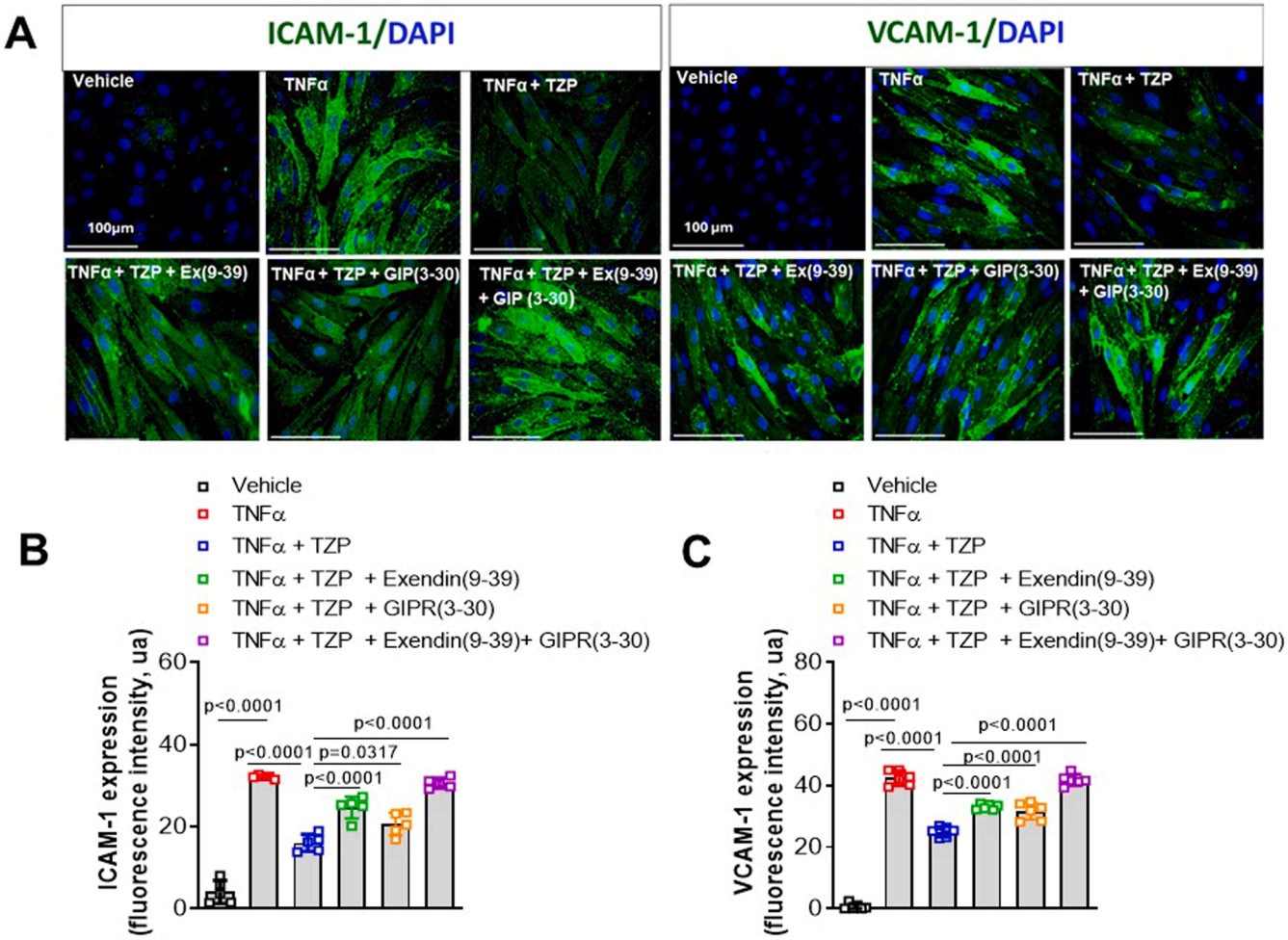

Fig. 2. Tirzepatide reduces TNFα-induced ICAM−1 and VCAM−1 expression in human endothelial cells. Cells were treated with TZP (100 nM) for 24 h and then stimulated with TNFα (20 ng/mL, 24 h). Specific plates were preincubated with exendin (9–39) (GLP−1R antagonist; 1 μM) and/or GIP (3−30) (GIPR antagonist; 1 μM) 1 h before TNFα treatment. **A** Representative immunofluorescence analysis of ICAM−1 and VCAM−1 expression (*green*) in HUVEC. Nuclei are counterstained with DAPI (*blue*). **B–C** Quantification of ICAM−1 and VCAM−1 expressed as fluorescence intensity (arbitrary units, ua). Data represent the mean ± SEM of 5–6 independent experiments. Data were analyzed by one-way ANOVA followed by Tukey *post hoc* test.

partially reversed this effect, simultaneous blockade of both GLP−1R and GIPR significantly abolished the suppressive effect of tirzepatide on NF-κB nuclear translocation ($p < 0.0001$, Fig. 4**A–B**). These findings were further validated by western blot analysis, which demonstrated that TNFα stimulation triggered significant phosphorylation of the p65 subunit ($p < 0.0001$, Fig. 4**C–D**). This was significantly attenuated by tirzepatide treatment ($p = 0.004$, Fig. 4**C–D**). In additional experiments, western blot analyses were performed to evaluate whether tirzepatide affected the activity of the AP−1 transcription factor pathway, as assessed by phosphorylation of c-Jun, a major component of the AP−1 complex. However, tirzepatide treatment did not alter TNFα-induced c-Jun phosphorylation ($p > 0.05$, Fig. 4**E–F**).

3.4. Tirzepatide treatment inhibits Ang-II-induced dissecting aneurysm formation

To investigate whether tirzepatide influences aneurysm development *in vivo*, *apoE*$^{-/-}$ mice were infused with Ang-II for 28 days to induce AAA. As shown in Fig. 5**A** and **B**, Ang-II infusion resulted in a significantly greater maximal external diameter of the suprarenal aorta compared with vehicle-infused controls (Ang-II: 2.37 ± 0.18 mm vs. vehicle: 0.91 ± 0.03 mm, $p < 0.0001$). While a 28-day treatment with 10 nmol/kg/day tirzepatide had no detectable effect on Ang-II–induced aortic dilation, the higher dose of 30 nmol/kg/day significantly reduced the maximal external suprarenal aortic diameter by 76% ($p < 0.0001$, Fig. 5**B**). Furthermore, according to the Daugherty classification system [27], the aneurysms induced by Ang-II were more severe than those in mice cotreated with 30 nmol/kg/day tirzepatide (Fig. 5**C**).

The impact of tirzepatide on mortality was also assessed. Compared to vehicle treated mice, within the initial 23 days of treatment, 41% of mice in both the Ang-II-infused group ($n = 5$) and the cotreated low-dose tirzepatide group ($n = 5$) died due to aortic rupture in the suprarenal abdominal region ($p = 0.013$), while mortality was reduced to 16% ($n = 2$) in mice cotreated with 30 nmol/kg/day of tirzepatide ($p = 0.179$, Fig. 5**D**). Furthermore, tirzepatide significantly reduced body weight and blood glucose levels in *apoE*$^{-/-}$ mice infused with Ang-II (Table I in the online-only Data Supplement). However, tirzepatide administration did not influence the Ang-II-induced elevation of blood pressure or the lipid profile (total cholesterol, HDL cholesterol, triglycerides) (Table I in the online-only Data Supplement).

Histological analysis of suprarenal aortic segments revealed that Ang-II infusion induced marked structural alterations (Fig. 6**A**), characterized by substantial degradation and fragmentation of the medial elastic laminae ($p = 0.005$, Fig. 6**B** and **D**) and a pronounced loss of vascular smooth muscle cells (VSMCs) within the media ($p < 0.0001$, Fig. 6**C** and **E**). These pathological changes were notably ameliorated in mice cotreated with tirzepatide, which preserved elastin architecture and attenuated medial VSMC depletion ($p = 0.033$ and $p < 0.0001$,

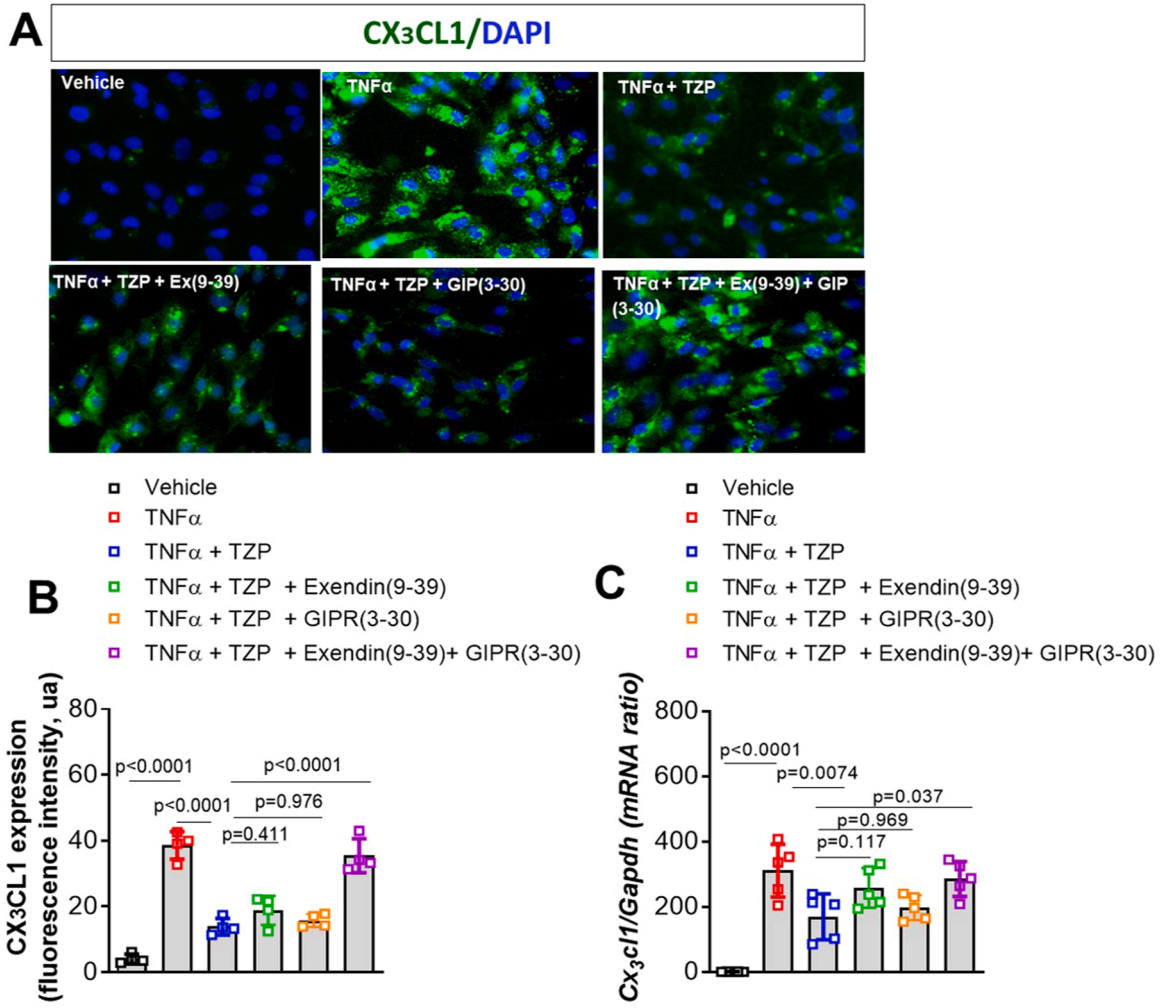

Fig. 3. Tirzepatide reduces TNFα-induced CX_3CL1/fractalkine expression in human endothelial cells. Cells were treated with TZP (100 nM) for 24 h and then stimulated with TNFα (20 ng/mL, 24 h). Specific plates were preincubated with exendin (9–39) (GLP−1R antagonist; 1 μM) and/or GIP (3−30) (GIPR antagonist; 1 μM) 1 h before TNFα treatment. **A** Representative immunofluorescence analysis of CX_3CL1 expression (*green*) in HUVEC. Nuclei are counterstained with DAPI (*blue*). **B** Quantification of CX_3CL1 expressed as fluorescence intensity (arbitrary units, ua). Data represent the mean ± SEM of 5–6 independent experiments. Data were analyzed by one-way ANOVA followed by Tukey *post hoc* test. **C** Analysis of *Cx3cl1* expression in suprarenal aortas. Data represent the mean ± SEM of the ratio between *Cx3cl1* gene and *Gapdh* gene expression (n = 4–5 animals/group). Data were analyzed by one-way ANOVA followed by Tukey *post hoc* test.

respectively; Fig. 6**C–D**).

Given the critical role of MMPs in extracellular matrix degradation and aortic wall remodeling in aortic aneurysm [32], we performed immunohistochemistry analysis for MMP−2 and MMP−9. Aortic expression of both MMP−2 ($p < 0.0001$, Fig. 6**F** and **H**) and MMP−9 ($p < 0.0001$, Fig. 6**G** and **I**) was significantly higher in Ang-II-infused mice than in vehicle-treated mice. Tirzepatide treatment significantly reduced the Ang-II-induced expression of both enzymes ($p < 0.0001$ for both, Fig. 6**H–I**). These findings were further supported by RT–PCR analysis. As shown in Fig. 6**J** and **K**, *Mmp−2* and *Mmp−9* mRNA levels in suprarenal aortas were significantly reduced in tirzepatide-treated mice ($p = 0.0014$ and $p = 0.0280$, respectively; Fig. 6**J** and **K**).

3.5. Tirzepatide reduces macrophage accumulation and neovascularization in dissecting AAA induced by Ang-II

Because AAA pathogenesis is driven by inflammation and angiogenesis [33,34], we assessed macrophage accumulation and microvessel density. In Ang-II-treated mice, we observed substantial macrophage accumulation within the medial and adventitial layers ($p < 0.0001$, Fig. 7**A** and **C**). This inflammatory response was reduced by 88% in mice cotreated with tirzepatide ($p < 0.0001$, Fig. 7**A** and **C**). Similarly, the high density of CD31 + microvessels observed in Ang-II-stimulated aortas ($p < 0.0001$, Fig. 7**B** and **D**) was markedly decreased by tirzepatide cotreatment ($p < 0.0001$, Fig. 7**B** and **D**). These histological findings were supported by mRNA analysis. The Ang-II–induced mRNA upregulation of *Mcp−1/Ccl2* ($p = 0.033$, Fig. 7**E**), *Rantes/Ccl5* ($p = 0.0003$, Fig. 7**F**), and *Vegf* ($p = 0.0256$, Fig. 7**G**) in suprarenal aortas was significantly attenuated in tirzepatide-treated mice ($p = 0.037$, $p = 0.006$, and $p = 0.0022$, respectively). In contrast, *Cx3cl1* mRNA expression was not significantly increased in Ang-II-infused suprarenal aortas compared with controls ($p > 0.05$, Fig. 7**H**), and tirzepatide treatment did not significantly modify its expression.

Finally, we confirmed the presence of both GLP−1R and GIPR in the suprarenal aortas of $apoE^{-/-}$ mice *via* western blot. Both receptors were detectable, and their expression levels remained unchanged regardless of Ang-II or tirzepatide treatment (Fig. 8**A–C**) ($p > 0.05$). Notably, complementary immunofluorescence studies demonstrated that GLP−1R and GIPR colocalize with both macrophages and endothelial cells within the suprarenal aortic wall (Fig. 8**D**). Given the well-established involvement of NF-κB signaling in AAA pathogenesis, we next investigated the impact of tirzepatide treatment on this pathway in suprarenal aneurysmal tissue. Compared with vehicle-treated controls,

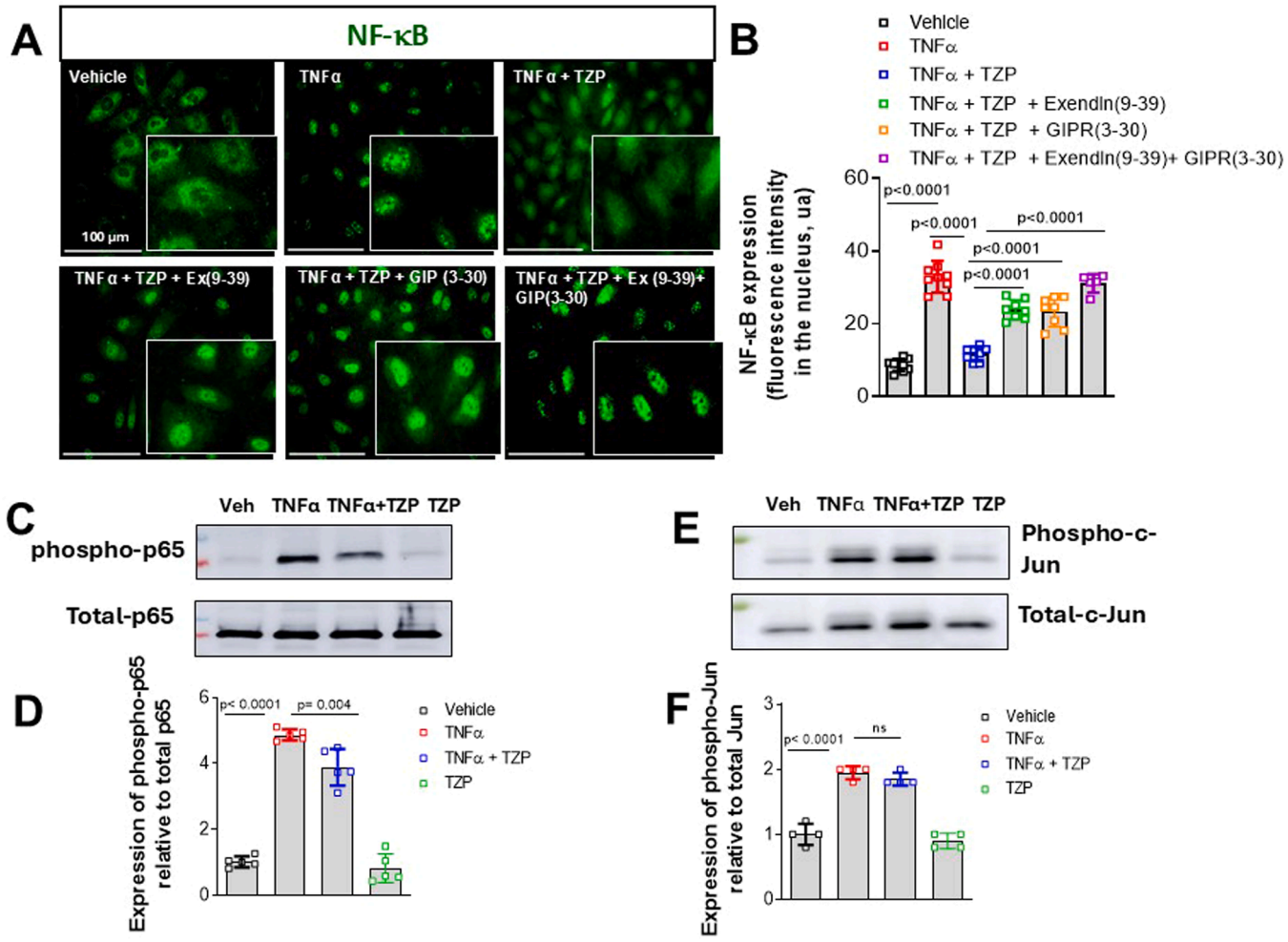

Fig. 4. Tirzepatide attenuates TNFα-induced NF-κB/p65 signaling in human endothelial cells. HUVEC were treated with TNFα (20 ng/mL) or vehicle for 30 min. Specific plates were pretreated with TZP (100 nM) 24 h before the stimulus. Similarly, specific TZP-treated cells were also pretreated with exendin (9–39) (GLP−1R antagonist; 1 μM) and/or GIP (3−30) (GIPR antagonist; 1 μM) 1 h before. **A**–**B** NF-κB expression in the nucleus was visualized and measured by immunofluorescence (scale bar = 100 μm). Data represent the mean ± SEM of 5–6 independent experiments. Data were analyzed by one-way ANOVA followed by Tukey *post hoc* test. **C** Phosphorylation of p65/NF-κB was analyzed by western blotting. Representative images are shown. **D** Densitometry analysis of phospho-p65 relative to total-p65 expression. Data represent the mean ± SEM of 5–6 independent experiments. Data were analyzed by one-way ANOVA followed by Tukey *post hoc* test. **E** Phosphorylation of c-Jun was analyzed by western blotting. Representative images are shown. **F** Densitometry analysis of phospho-c-Jun relative to total-c-Jun expression. Data represent the mean ± SEM of 4 independent experiments. Data were analyzed by one-way ANOVA followed by Tukey *post hoc* test.

suprarenal aortas from Ang-II-infused apoE$^{-/-}$ mice exhibited significantly increased phosphorylation of p65 (Fig. 8**E** and **F**), indicating activation of NF-κB signalling ($p = 0.0016$). Notably, tirzepatide cotreatment markedly reduced p65 phosphorylation in suprarenal aortic tissue, suggesting attenuation of NF-κB pathway activation ($p = 0.0217$).

4. Discussion

Tirzepatide, currently the only approved dual GLP−1R/GIPR agonist, has demonstrated impressive clinical efficacy in patients with T2D and for chronic weight management in adults with obesity or overweight who present with weight-related comorbidities [13,14,35–37]. Beyond its metabolic indications, emerging clinical and preclinical evidence suggests that tirzepatide may offer therapeutic benefits in nondiabetic cardiovascular contexts, specifically regarding myocardial infarction [18,38,39] and heart failure [40–42]. However, the direct impact of dual GLP−1R/GIPR agonism on endothelial dysfunction and AAA pathogenesis remains unexplored.

Endothelial dysfunction serves as a critical predictor of cardiovascular events and plays a pivotal role in the early pathogenesis of AAA [5]. TNFα is a key mediator of vascular inflammation and has been consistently reported to be upregulated in Ang-II–induced abdominal aortic aneurysm models [43,44], where it contributes to macrophage accumulation and increased vascular inflammation. In our *in vitro* studies, TNFα stimulation of human endothelial cells induced a dysfunctional phenotype characterized by enhanced cell adhesion molecule (VCAM−1 and ICAM−1) and fractalkine/CX_3CL1 expression and subsequent increased leukocyte adhesion. Pharmacological activation of either GLP−1R or GIPR partially attenuated these inflammatory responses, whereas dual GLP−1R/GIPR agonism produced a more pronounced inhibitory effect, suggesting additive or synergistic interactions between the two pathways. Consistently, blockade of both receptors reversed the protective effects of tirzepatide, while single receptor antagonism only partially restored TNFα-induced CAM/fractalkine expression and leukocyte recruitment. These findings indicate that GLP−1R and GIPR signaling contribute individually to the anti-inflammatory effects of tirzepatide, but co-activation is necessary to fully suppress endothelial inflammation, highlighting the synergistic relevance of dual agonism in mediating vascular protection. Consistent with our findings, recent clinical data from patients with T2D have reported that a 26-week regimen of tirzepatide reduces endothelial

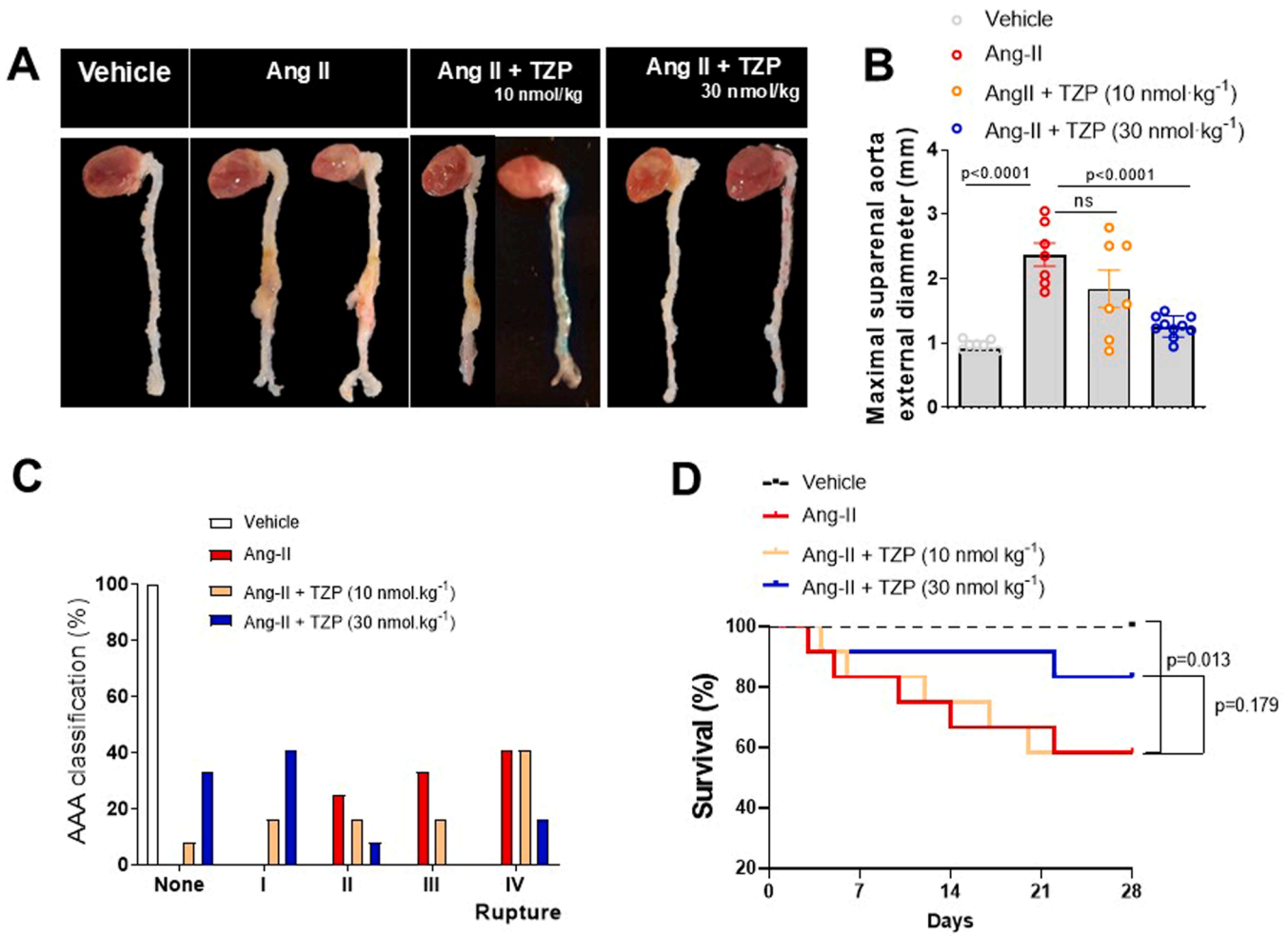

Fig. 5. Effect of tirzepatide treatment on Ang-II-induced dissecting AAA in apoE$^{-/-}$ mice. Mice were treated with vehicle, Ang-II, Ang-II + TZP (10 or 30 nmol/kg) for 28 days. **A** Representative micrographs displaying macroscopic features of aortas. **B** Maximal external diameter of suprarenal aorta (mm) was measured by morphometry at day 28. Data represent the mean ± SEM (n = 7–10 animals/group). Data were analyzed by one-way ANOVA followed by Tukey *post hoc* test. **C** Aneurysm severity (stage I to IV) was scored. Stage IV was attributed to ruptured aneurysms. **D** Kaplan-Meier curves of survival free from abdominal aneurysm rupture. Data represent the mean ± SEM. Data were analyzed by one-way ANOVA followed by Tukey *post hoc* test.

dysfunction and lowers several inflammatory biomarkers associated with cardiovascular risk, including ICAM−1, YKL−40 (also known as chitinase−3-like-protein−1), leptin, and growth differentiation factor−15 [16]. Furthermore, while the GLP−1R agonist liraglutide has previously been shown to decrease TNFα-induced VCAM−1 and ICAM−1 expression in preclinical models [45,46], our findings suggest that the protective effects of dual GLP−1R/GIPR agonism on AAA are driven, at least in part, by a potent anti-inflammatory action on the vascular endothelium.

We report the first evidence that chronic administration of tirzepatide over 28 days effectively decreases Ang-II-induced aortic dilatation and AAA formation. These beneficial effects were accompanied by a significant reduction in macrophage accumulation within the lesions and a downregulation of key proinflammatory chemokines, such as *Mcp−1/Ccl2* and *Rantes/Ccl5,* in the aorta wall. This aligns with previous findings showing an upregulation of these chemokines in both human AAA and animal models [33,34,47–49]. Our observations are also consistent with reports that liraglutide reduces Ang-II-induced AAA by inhibiting M1 macrophage polarization (57). Interestingly, retrospective clinical data from 1401 matched patients with T2D and 336 matched patients without T2D with unruptured AAA have associated GLP−1 receptor agonist prescriptions with lower rates of mortality and AAA repair over a 5-year follow-up period, suggesting potential benefits of GLP−1RAs in AAA management [50]. Additionally, the anti-atherogenic effects of GLP−1 and GIP and their selective receptor agonists are well documented in murine models [51–55]. For instance, active forms of GLP−1 and GIP suppress macrophage accumulation into the aortic wall and prevent atherosclerotic lesion development in *apoE*$^{-/-}$ mice [55]. Similarly, liraglutide reduces atheroma development and several inflammatory mediators (TNFα, IL−1β, MCP−1/CCL2) in the vascular wall [52]. While the specific effects of GIP on vascular inflammation are less established, evidence suggests it also reduces macrophage accumulation in atherosclerosis models [56]. Beyond the pancreas, GLP−1R and GIPR are expressed in various tissues and vascular cells, including the endothelium [57], macrophages [58], immune cells [59], as well as the aorta [59–62]. This expression pattern suggests a pivotal role for these receptors in vascular biology. In the present study, we confirmed the presence of both GLP−1R and GIPR in macrophages and vascular endothelial cells.

Although macrophage accumulation was quantified using MAC−3 immunostaining, this approach did not permit discrimination between resident and monocyte-derived macrophages or characterization of macrophage phenotype. Current evidence indicates that macrophages in AAA comprise a heterogeneous population and that the majority of cells accumulating within the aneurysmal wall are derived from circulating monocytes rather than resident macrophage populations [7]. In addition, macrophages in AAA can adopt diverse functional states, including pro-inflammatory and reparative phenotypes, which contribute

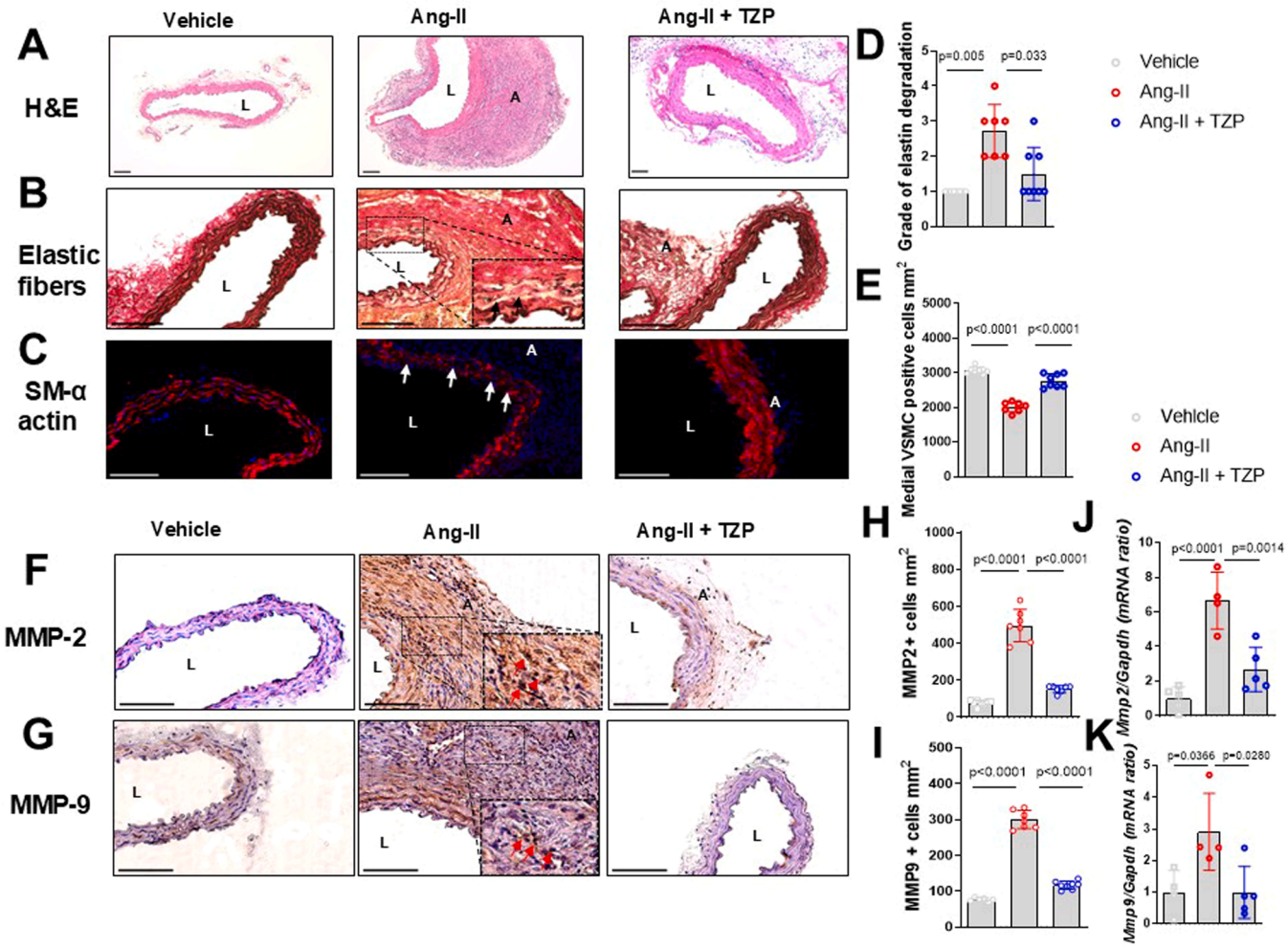

Fig. 6. Tirzepatide effects on elastic fibers, VSMCs, and MMPs in aortas of Ang-II-infused *apoE*$^{-/-}$ mice. A Representative photomicrographs of hematoxylin and eosin (H&E) staining. **B** Representative images of elastin fiber immunohistochemical stain (Weigert Van Gieson); arrows show the sites of elastin destruction, with higher magnifications of vessel areas depicted in the right panels. **C** Representative immunostaining of smooth muscle α-actin (*red*); nuclei were stained with DAPI (*blue*); arrows show the sites of medial smooth muscle cells loss. **D** The severity of elastin degradation was semiquantified as: grade 1, no degradation; grade 2, mild degradation; grade 3, severe degradation; and grade 4, presence of aortic rupture. Data represent the mean ± SEM (n = 7–8 animals/group). **E** Quantitative data for VSMC^{+} cells per mm^2 in suprarenal aortic sections. Data represent the mean ± SEM (n = 7–8 animals/group). Data were analyzed by Kruskal-Wallis followed by Dunn's *post hoc* test. **F–G** Representative immunohistochemical staining for MMP−2 and MMP−9; arrows show positive staining. **H–I** Quantitative data for MMP−2^{+} MMP−9^{+} cells per mm^2 in suprarenal aortic sections. **J-K** Analysis of *Mmp−2 and Mmp−9* expression in suprarenal aortas. Data represent the mean ± SEM of the ratio between *each* gene and *Gapdh* gene expression (n = 4–5 animals/group). Data were analyzed by one-way ANOVA followed by Tukey *post hoc* test. Lumen and adventitial regions are indicated as L and A, respectively. Scale bar = 100 μm. Data represent the mean ± SEM (n = 7–8 animals/group). Data were analyzed by one-way ANOVA followed by *Tukey post hoc* test.

differentially to aneurysm progression and tissue remodeling [7,63]. Therefore, the reduction in MAC−3-positive cells observed following tirzepatide treatment likely reflects attenuation of inflammatory cell recruitment and/or expansion within the lesion. However, the present study cannot determine whether tirzepatide preferentially affects specific macrophage subsets or phenotypic states. Given the emerging roles of distinct macrophage populations in aneurysm progression and repair [7,63], further studies are warranted to define the effects of tirzepatide on macrophage origin, polarization, and function during AAA development.

In a clinical context, the SUMMIT trial recently reported that tirzepatide reduced circulatory volume–pressure overload and systemic inflammation while mitigating cardiovascular-kidney end-organ injury in patients with obesity and heart failure with preserved ejection fraction [64]. These findings provide critical insights into the pleiotropic cardiovascular benefits of this agent. Correspondingly, preclinical models of myocardial infarction have shown that chronic treatment with tirzepatide reduces mortality, limits infarct size and inflammatory infiltration, and restores left ventricular function [39]. Furthermore, tirzepatide was recently shown to attenuate doxorubicin-induced cardiotoxicity by reducing macrophage accumulation and the expression of several proinflammatory markers, including IL−1β, IL−6 and TNFα, in the myocardium [65]. By utilizing a pharmacological approach, our study further demonstrates the efficacy of tirzepatide in attenuating AAA and provides additional evidence for the combined roles of GLP−1R and GIPR in modulating the immune and inflammatory profile of the vascular wall.

The pathogenesis of AAA involves a complex interplay between endothelial cells, SMCs, and infiltrating immune cells – particularly macrophages – which release MMPs that drive elastin degradation and medial SMC apoptosis [32]. In our study, tirzepatide-treated mice exhibited significantly reduced medial elastin destruction and downregulated expression of MMP−2 and MMP−9 in suprarenal aortas. These findings align with data showing that GLP−1R activation *via* liraglutide reduces both MMP expression and elastin degradation, and attenuates AAA formation induced by elastase [66]. Similarly, *in vitro*

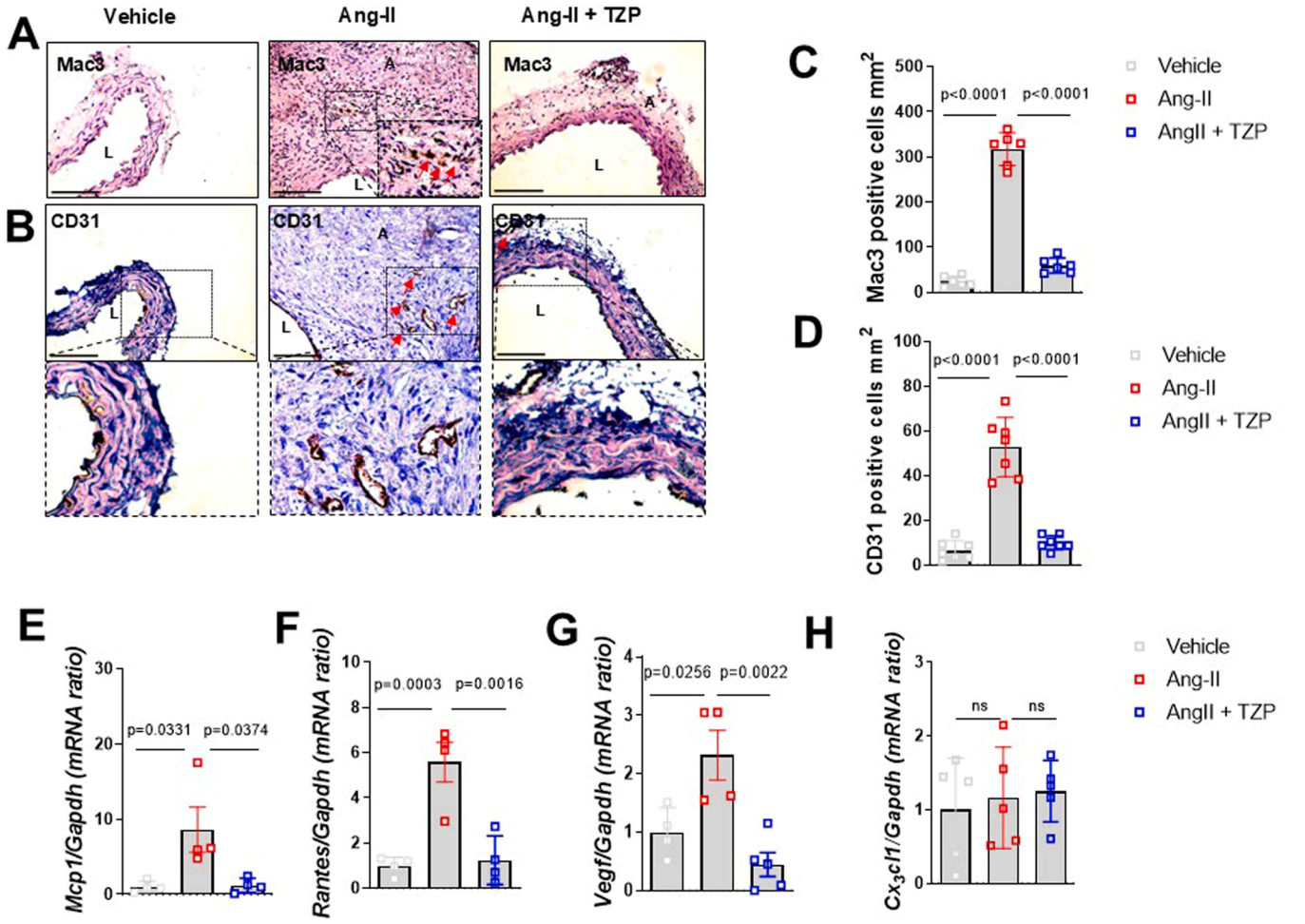

Fig. 7. Tirzepatide effects on macrophage infiltration, neovascularization and chemokine expression in Ang-II-infused *apoE*$^{-/-}$ mice aortas. A–B Representative immunohistochemical staining of Mac3^{+} cells and CD31^{+} microvessels. **C–D** Quantitative data for Mac3^{+} cells CD31^{+} microvessels per mm^{2} in suprarenal aortic sections. Lumen and adventitial regions are indicated as L and A, respectively. Data represent the mean ± SEM (n = 6–7 animals/group). Scale bar = 100 μm. Data were analyzed by one-way ANOVA followed by Tukey *post hoc* test. **E–H** Analysis of (E) *Mcp−1/Ccl2*, (F) *Rantes/Ccl5*, (G) *Vegf* and (H) *Cx3cl1* expression in suprarenal aortas. Data represent the mean ± SEM of the ratio between each gene and *Gapdh* gene expression (n = 4–5 animals/group). Data were analyzed by one-way ANOVA followed by Tukey *post hoc* test.

studies showed that GIP treatment significantly prevents endotoxin-induced MMP−9 secretion in murine macrophages [56]. Collectively, these results suggest that dual GLP−1R/GIPR agonism plays a crucial role in preserving vascular structural integrity.

Enhanced neovessel formation within the aortic media is a hallmark of AAA progression and rupture [67]. Dysregulation of growth factors and proangiogenic chemokines contributes to this neovascularization [67], and MCP−1/CCL2, RANTES/CCL5, and VEGF have been identified as potential angiogenic factors in the response exerted by Ang-II [33, 68]. Currently, there is limited direct evidence on whether GLP−1R or GIPR agonists could modulate angiogenic response in the arterial wall in AAA. Our study provides some of the first evidence that tirzepatide reduces neovascularization and *Vegf* levels in the suprarenal aorta. This effect might stem from a direct effect on endothelial cells or a secondary reduction in macrophage infiltration, as macrophages are the primary source of VEGF. Thus, it is highly probable that the anti-inflammatory effects of tirzepatide indirectly suppress pathological angiogenesis in the context of AAA.

The underlying mechanisms involved in the beneficial actions of tirzepatide have been associated with antihypertensive effects. While the SURPASS clinical program observed systolic blood pressure reductions in patients with T2D [69], tirzepatide treatment in our model had no significant effect on Ang-II-induced hypertension. This indicates that, in this experimental setting, the protective effects of dual GLP−1R/GIPR agonism on vascular aneurysmal formation are blood pressure-independent, consistent with a prior report of an Ang-II-induced AAA model [70].

NF-κB activation is a central driver of cytokine/chemokine upregulation, CAM expression, and leukocyte recruitment during AAA development [34,47]. Activation of GLP−1R and GIPR engages multiple intracellular pathways that may contribute to suppression of NF-kappa B. These include increased cyclic AMP (cAMP) levels and subsequent activation of protein kinase A (PKA), as well as engagement of PI3K/Akt and AMP-activated protein kinase (AMPK) signaling, all of which have been implicated in reducing inflammatory responses and NF-κB activity in preclinical and clinical contexts [71,72]. We found that tirzepatide attenuated human endothelial cell dysfunction, mitigated VCAM−1/ICAM−1 expression and MCP−1 and RANTES release, and decreased the phosphorylation of NF-κB/p65 in endothelial cells induced by TNFα. In contrast, tirzepatide did not significantly affect TNFα-induced c-Jun phosphorylation, suggesting that its anti-inflammatory actions are mediated predominantly through modulation of NF-κB signaling rather than AP−1 pathway inhibition. These findings are supported by evidence that GLP−1 R selective agonism inhibits the NF-κB pathway in endothelial cells [73], and that GIP reduces lipopolysaccharide-induced IL−6 secretion and MMP−9 activity

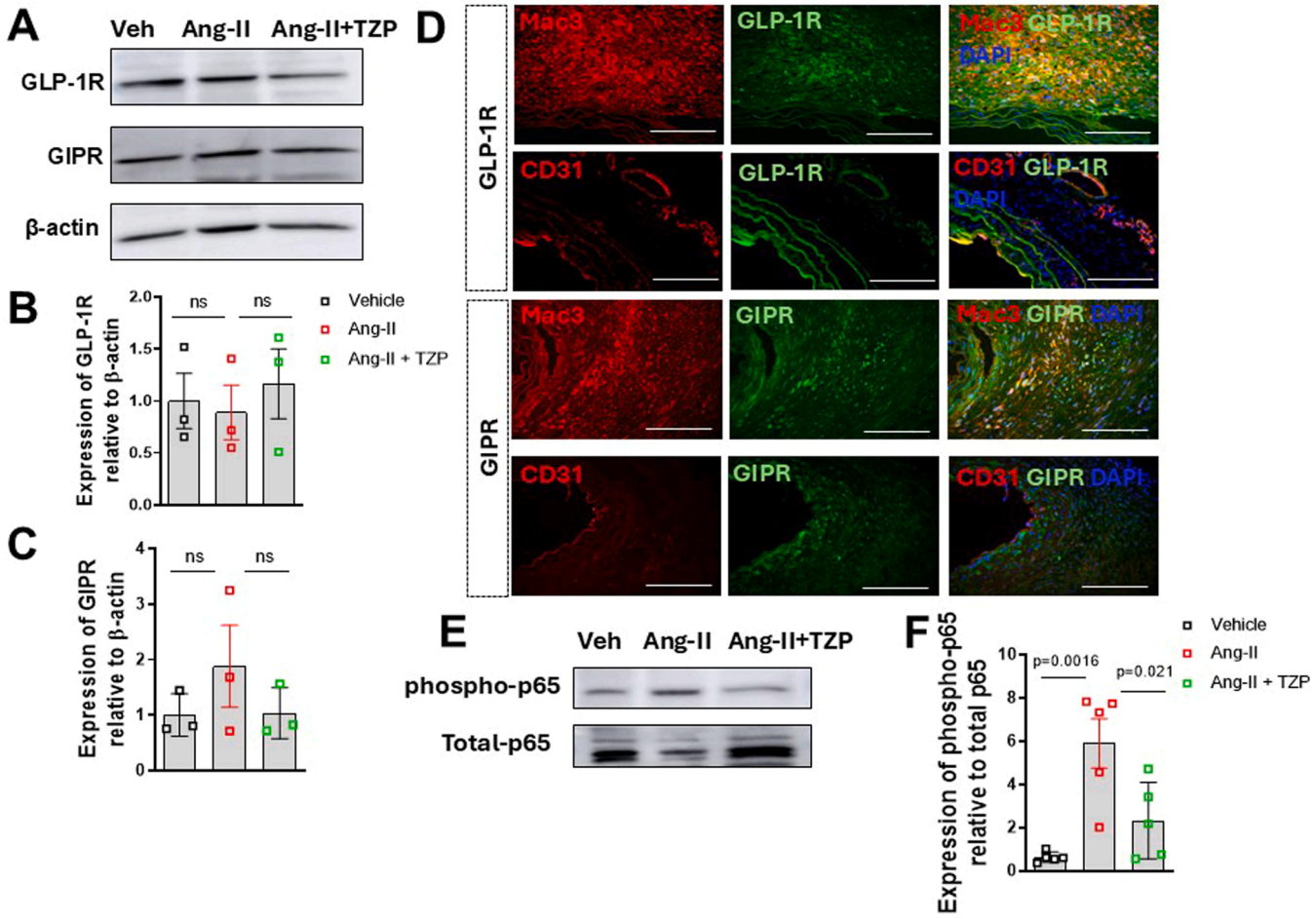

Fig. 8. GLP−1R and GIPR expression is detected in the suprarenal aortas of *apoE*$^{-/-}$ mice. A Representative images of western blot analysis of GLP−1R and GIPR expression in aortas. **B–C** Protein expression quantification for GLP−1R and GIPR protein relative to β-actin in suprarenal aortas of mice. Data represent the mean ± SEM (n = 3 animals/group). Data were analyzed by one-way ANOVA followed by Tukey *post hoc* test. **D** Representative images of colocalization of GLP−1R and GIPR in macrophages (Mac3) and endothelial cells (CD31 +). Immunoreactivity was visualized using Alexa Fluor 488 (*green*) and Alexa Fluor 594 (*red*) secondary antibodies. Nuclei were stained with DAPI (*blue*). Scale bar = 100 μm. **E** Phosphorylation of p65/NF-κB was analyzed by western blotting in the aortas. Representative images are shown. **F** Densitometry analysis of phospho-p65 relative to total-p65 expression in the aortas. Data represent the mean ± SEM of 5 independent experiments. Data were analyzed by one-way ANOVA followed by Tukey *post hoc* test.

through NF-κB inhibition in macrophages [56]. Taken together, the vascular benefits of tirzepatide indicate that impaired NF-κB pathway activation attenuates the synthesis of proinflammatory molecules, ultimately mitigating endothelial dysfunction. Our data further confirm that both GIPR and GLP−1R contribute to these potent anti-inflammatory effects.

Limitations of the present study should be considered. Due to the higher prevalence of AAA in males, both in humans [74] and in experimental models [10,75,76], all experiments were conducted exclusively in male mice. In the original characterization of the suprarenal AAA model, Manning *et al.* (2002) reported that when female mice were studied, only 20–33% developed aneurysms under comparable experimental conditions [76]. Therefore, the use of male animals is considered standard practice to ensure model robustness and reproducibility. Nevertheless, the biological mechanisms underlying sex-dependent differences in aneurysm susceptibility remain incompletely understood and warrant further investigation. Another potential limitation of our study is the use of HUVEC for *in vitro* experiments rather than arterial endothelial cells, such as human aortic endothelial cells (HAEC) or human umbilical artery endothelial cells (HUAEC). While HUVEC are widely used due to their robust growth, and well-characterized responses to inflammatory stimuli and shear stress, venous endothelial cells differ from arterial endothelial cells in baseline gene expression, sensitivity to flow, and inflammatory signaling. Therefore, while our HUVEC-based findings provide a valuable mechanistic insight into GLP−1R/GIPR-mediated modulation of endothelial–leukocyte interactions, caution should be exercised when extrapolating these results to endothelial biology in AAA. Future studies using human aortic endothelial cells will be important to confirm the vascular relevance of these observations in the context of AAA pathophysiology.

5. Conclusions

In conclusion, the present study provides the first evidence that dual GLP−1R/GIPR agonism significantly reduces endothelial dysfunction and attenuates AAA formation in a murine model. The pleiotropic effects of tirzepatide – specifically the mitigation of vascular inflammation, pathological neovascularization, and MMP dysregulation – demonstrate that dual receptor activation effectively preserves aortic structural integrity. These findings suggest that therapeutic dual GLP−1R/GIPR agonism represents a viable clinical strategy to limit AAA progression and its associated mortality. Furthermore, our results highlight a promising role for tirzepatide beyond metabolic control, opening a novel avenue of cardiovascular research that warrants further investigation in clinical trials.

Abbreviations

AAA, abdominal aortic aneurysm; Ang-II, angiotensin-II; *apoE*, apolipoprotein E; BSA, bovine serum albumin; CAM, cell adhesion molecule; ELISA, enzyme-linked immunosorbent assay; FBS, fetal bovine serum; GIP, glucose-dependent insulinotropic peptide; GIPR, glucose-dependent insulinotropic peptide receptor; GLP−1, glucagon-like peptide−1; GLP−1R, glucagon-like peptide−1 receptor; H&E, hematoxylin and eosin; HDL-C, high-density lipoprotein cholesterol; HUVEC, human umbilical vein endothelial cells; HRP, horseradish peroxidase; ICAM−1, intercellular adhesion molecule−1; MCP−1, monocyte chemoattractant protein; MMP, matrix metalloproteinase; NF-κB, nuclear factor-kappa B; PBS, phosphate-buffered saline; RANTES, regulated on activation normal T-cell expressed and secreted; SMC, smooth muscle cell; T2D, type 2 diabetes; TNFα, tumor necrosis factor-α; TBS, tris-buffered saline; TZP, tirzepatide; VCAM−1, vascular cell adhesion molecule−1; VEGF, vascular endothelial growth factor.

Ethics approval

This study involved experimental procedures in animals. All animal experiments were reviewed and approved by the Ethics Review Committee of the School of Medicine, University of Valencia, and the Valencian regional authorities (ref. VSC187–186 PEA−0260). All animal procedures complied with the ARRIVE (Animal Research: Reporting of In Vivo Experiments) guidelines, the EU Directive 2010/63/EU for the protection of animals used for scientific purposes, and the EU Commission Recommendation 2007/526/EC on guidelines for the accommodation and care of animals used for experimental and other scientific purposes.

Funding

This work was supported by the Instituto de Salud Carlos III (ISCIII) [grant numbers PI21–00220, PI25–01315], the Spanish Ministry of Science and Innovation [grant number PID2023–152677OB-I00], the Generalitat Valenciana [Grant Numbers CIPROM/2022/45, CIGE/2023/073] and the European Regional Development Fund (FEDER). Álvaro Gómez-Martín and Elena Domingo were funded by a pre-doctoral grant and a post-doctoral grant, respectively, from the Generalitat Valenciana [grant number CIPROM/2022/45]. Patrice Marques was funded by a post-doctoral grant from the ISCIII [grant number CD22/00045].

CRediT authorship contribution statement

Laura Piqueras: Writing – original draft, Project administration, Methodology, Investigation, Funding acquisition, Conceptualization. **Sanz Maria-Jesus:** Writing – review & editing, Funding acquisition, Conceptualization. **José T Real:** Writing – review & editing, Funding acquisition. **Cristina Arce-Recatalá:** Methodology, Investigation, Formal analysis. **Patrice Marques:** Writing – review & editing, Formal analysis. **Álvaro Gómez-Martín:** Methodology, Investigation, Formal analysis. **Ángela Vea:** Methodology, Investigation, Formal analysis. **Blanca Alabadi:** Methodology, Investigation, Formal analysis. **Elena Domingo:** Methodology, Investigation, Formal analysis.

Declaration of Competing Interest

The authors declare that they have no known competing financial interests or personal relationships that could have appeared to influence the work reported in this paper.

Appendix A. Supporting information

Supplementary data associated with this article can be found in the online version at doi:10.1016/j.phrs.2026.108321.

Data availability

Data will be made available on request.

References

[1] M.P. Calgi, J.S. McNeil, Abdominal aortic aneurysms (etiology, epidemiology, and natural history), Anesthesiol. Clin. 40 (4) (2022) 657–669, https://doi.org/10.1016/j.anclin.2022.08.010.
[2] S.H. Forsdahl, K. Singh, S. Solberg, B.K. Jacobsen, Risk factors for abdominal aortic aneurysms: a 7-year prospective study: the Tromsø Study, 1994-2001, Circulation 119 (16) (2009) 2202–2208, https://doi.org/10.1161/circulationaha.108.817619.
[3] R.A. Chang, N.F. Rossi, Intermittent cocaine use associated with recurrent dissection of the thoracic and abdominal aorta, Chest 108 (6) (1995) 1758–1762, https://doi.org/10.1378/chest.108.6.1758.
[4] J. Golledge, S. Thanigaimani, J.T. Powell, P.S. Tsao, Pathogenesis and management of abdominal aortic aneurysm, Eur. Heart J. 44 (29) (2023) 2682–2697, https://doi.org/10.1093/eurheartj/ehad386.
[5] E. DeRoo, A. Stranz, H. Yang, M. Hsieh, C. Se, T. Zhou, Endothelial dysfunction in the pathogenesis of abdominal aortic aneurysm, Biomolecules 12 (4) (2022) 509, https://doi.org/10.3390/biom12040509.
[6] G. Siasos, K. Mourouzis, E. Oikonomou, S. Tsalamandris, V. Tsigkou, K. Vlasis, et al., The role of endothelial dysfunction in aortic aneurysms, Curr. Pharm. Des. 21 (28) (2015) 4016–4034, https://doi.org/10.2174/1381612821666150826094156.
[7] J. Raffort, F. Lareyre, M. Clément, R. Hassen-Khodja, G. Chinetti, Z. Mallat, Monocytes and macrophages in abdominal aortic aneurysm, Nat. Rev. Cardiol. 14 (8) (2017) 457–471, https://doi.org/10.1038/nrcardio.2017.52.
[8] A. Daugherty, L. Cassis, Angiotensin II and abdominal aortic aneurysms, Curr. Hypertens. Rep. 6 (6) (2004) 442–446, https://doi.org/10.1007/s11906-004-0038-0.
[9] L. Piqueras, M.J. Sanz, Angiotensin II and leukocyte trafficking: New insights for an old vascular mediator. Role of redox-signaling pathways, Free. Radic. Biol. Med. 157 (2020) 38–54, https://doi.org/10.1016/j.freeradbiomed.2020.02.002.
[10] A. Daugherty, M.W. Manning, L.A. Cassis, Angiotensin II promotes atherosclerotic lesions and aneurysms in apolipoprotein E-deficient mice, J. Clin. Invest. 105 (11) (2000) 1605–1612, https://doi.org/10.1172/jci7818.
[11] A. Daugherty, L. Cassis, Chronic angiotensin II infusion promotes atherogenesis in low density lipoprotein receptor -/- mice, Ann. N. Y Acad. Sci. 892 (1999) 108–118, https://doi.org/10.1111/j.1749-6632.1999.tb07789.x.
[12] R.J. Samms, M.P. Coghlan, K.W. Sloop, How May GIP Enhance the Therapeutic Efficacy of GLP-1? Trends Endocrinol. Metab. 31 (6) (2020) 410–421, https://doi.org/10.1016/j.tem.2020.02.006.
[13] J.P. Frias, M.A. Nauck, J. Van, M.E. Kutner, X. Cui, C. Benson, et al., Efficacy and safety of LY3298176, a novel dual GIP and GLP-1 receptor agonist, in patients with type 2 diabetes: a randomised, placebo-controlled and active comparator-controlled phase 2 trial, Lancet 392 (10160) (2018) 2180–2193, https://doi.org/10.1016/s0140-6736(18)32260-8.
[14] J.P. Frías, M.J. Davies, J. Rosenstock, F.C. Pérez Manghi, L. Fernández Landó, B. K. Bergman, et al., Tirzepatide versus Semaglutide Once Weekly in Patients with Type 2 Diabetes, N. Engl. J. Med. 385 (6) (2021) 503–515, https://doi.org/10.1056/NEJMoa2107519.
[15] R. Loomba, M.L. Hartman, E.J. Lawitz, R. Vuppalanchi, J. Boursier, E. Bugianesi, et al., Tirzepatide for Metabolic Dysfunction-Associated Steatohepatitis with Liver Fibrosis, N. Engl. J. Med. 391 (4) (2024) 299–310, https://doi.org/10.1056/NEJMoa2401943.
[16] J.M. Wilson, Y. Lin, M.J. Luo, G. Considine, A.L. Cox, L.M. Bowsman, et al., The dual glucose-dependent insulinotropic polypeptide and glucagon-like peptide-1 receptor agonist tirzepatide improves cardiovascular risk biomarkers in patients with type 2 diabetes: A post hoc analysis, Diabetes Obes. Metab. 24 (1) (2022) 148–153, https://doi.org/10.1111/dom.14553.
[17] E.R. Hankosky, H. Wang, L.M. Neff, H. Kan, F. Wang, N.N. Ahmad, et al., Tirzepatide reduces the predicted risk of atherosclerotic cardiovascular disease and improves cardiometabolic risk factors in adults with obesity or overweight: SURMOUNT-1 post hoc analysis, Diabetes Obes. Metab. 26 (1) (2024) 319–328, https://doi.org/10.1111/dom.15318.
[18] M.H. Bin Abdul Malik, N.N. Khan, M.J. Chowdhari, M.K. Rafiq, M. Ali, S. Lnu, et al., Evaluating the Impact of Tirzepatide on Clinical Outcomes in Patients With Heart Failure, Cureus 17 (4) (2025) e82118, https://doi.org/10.7759/cureus.82118.
[19] E.A. Jaffe, R.L. Nachman, C.G. Becker, C.R. Minick, Culture of human endothelial cells derived from umbilical veins. Identification by morphologic and immunologic criteria, J. Clin. Invest. 52 (11) (1973) 2745–2756, https://doi.org/10.1172/jci107470.
[20] L. Hueso, P. Marques, B. Morant, H. Gonzalez-Navarro, J. Ortega, J.T. Real, et al., CCL17 and CCL22 chemokines are upregulated in human obesity and play a role in vascular dysfunction, Front. Endocrinol. (Lausanne) 14 (2023) 1154158, https://doi.org/10.3389/fendo.2023.1154158.
[21] D.J. Goetz, D.M. Greif, J. Shen, F.W. Luscinskas, Cell-cell adhesive interactions in an in vitro flow chamber, Methods Mol. Biol. 96 (1999) 137–145, https://doi.org/10.1385/1-59259-258-9:137.

[22] S.A. Parsons, C. Jurzinsky, S.L. Cuvelier, K.D. Patel, Studying leukocyte recruitment under flow conditions, Methods Mol. Biol. 946 (2013) 285–300, https://doi.org/10.1007/978-1-62703-128-8_18.
[23] K.D. Patel, Mechanisms of selective leukocyte recruitment from whole blood on cytokine-activated endothelial cells under flow conditions, J. Immunol. 162 (10) (1999) 6209–6216.
[24] T. Coskun, K.W. Sloop, C. Loghin, J. Alsina-Fernandez, S. Urva, K.B. Bokvist, et al., LY3298176, a novel dual GIP and GLP-1 receptor agonist for the treatment of type 2 diabetes mellitus: From discovery to clinical proof of concept, Mol. Metab. 18 (2018) 3–14, https://doi.org/10.1016/j.molmet.2018.09.009.
[25] S. Urva, T. Coskun, C. Loghin, X. Cui, E. Beebe, L. O'Farrell, et al., The novel dual glucose-dependent insulinotropic polypeptide and glucagon-like peptide-1 (GLP-1) receptor agonist tirzepatide transiently delays gastric emptying similarly to selective long-acting GLP-1 receptor agonists, Diabetes Obes. Metab. 22 (10) (2020) 1886–1891, https://doi.org/10.1111/dom.14110.
[26] A. Daugherty, D. Rateri, L. Hong, A. Balakrishnan, Measuring blood pressure in mice using volume pressure recording, a tail-cuff method, J. Vis. Exp. (27) (2009) 1291, https://doi.org/10.3791/1291.
[27] A. Daugherty, M.W. Manning, L.A. Cassis, Antagonism of AT2 receptors augments angiotensin II-induced abdominal aortic aneurysms and atherosclerosis, Br. J. Pharmacol. 134 (4) (2001) 865–870, https://doi.org/10.1038/sj.bjp.0704331.
[28] R. Benedé-Ubieto, O. Estévez-Vázquez, P. Ramadori, F.J. Cubero, Y.A. Nevzorova, Guidelines and Considerations for Metabolic Tolerance Tests in Mice. *Diabetes Metab Syndr Obes* 13 (2020) 439–450, https://doi.org/10.2147/dmso.S234665.
[29] J. Sun, G.K. Sukhova, M. Yang, P.J. Wolters, L.A. MacFarlane, P. Libby, et al., Mast cells modulate the pathogenesis of elastase-induced abdominal aortic aneurysms in mice, J. Clin. Invest. 117 (11) (2007) 3359–3368, https://doi.org/10.1172/jci31311.
[30] C. Rush, M. Nyara, J.V. Moxon, A. Trollope, B. Cullen, J. Golledge, Whole genome expression analysis within the angiotensin II-apolipoprotein E deficient mouse model of abdominal aortic aneurysm, BMC Genom. 10 (2009) 298, https://doi.org/10.1186/1471-2164-10-298.
[31] H. Zhang, Y. Park, J. Wu, X. Chen, S. Lee, J. Yang, et al., Role of TNF-alpha in vascular dysfunction, Clin. Sci. (Lond.) 116 (3) (2009) 219–230, https://doi.org/10.1042/cs20080196.
[32] D. Domagała, K. Data, H. Szyller, M. Farzaneh, P. Mozdziak, S. Woźniak, et al., Cellular, Molecular and Clinical Aspects of Aortic Aneurysm-Vascular Physiology and Pathophysiology, Cells 13 (3) (2024) 274, https://doi.org/10.3390/cells13030274.
[33] P. Escudero, A. Navarro, C. Ferrando, E. Furio, H. Gonzalez-Navarro, M. Juez, et al., Combined treatment with bexarotene and rosuvastatin reduces angiotensin-II-induced abdominal aortic aneurysm in apoE(-/-) mice and angiogenesis, Br. J. Pharmacol. 172 (12) (2015) 2946–2960, https://doi.org/10.1111/bph.13098.
[34] S. Martorell, L. Hueso, H. Gonzalez-Navarro, A. Collado, M.J. Sanz, L. Piqueras, Vitamin D Receptor Activation Reduces Angiotensin-II-Induced Dissecting Abdominal Aortic Aneurysm in Apolipoprotein E-Knockout Mice, Arterioscler. Thromb. Vasc. Biol. 36 (8) (2016) 1587–1597, https://doi.org/10.1161/atvbaha.116.307530.
[35] D. Dahl, Y. Onishi, P. Norwood, R. Huh, R. Bray, H. Patel, et al., Effect of Subcutaneous Tirzepatide vs Placebo Added to Titrated Insulin Glargine on Glycemic Control in Patients With Type 2 Diabetes: The SURPASS-5 Randomized Clinical Trial, Jama 327 (6) (2022) 534–545, https://doi.org/10.1001/jama.2022.0078.
[36] S. Del Prato, S.E. Kahn, I. Pavo, G.J. Weerakkody, Z. Yang, J. Doupis, et al., Tirzepatide versus insulin glargine in type 2 diabetes and increased cardiovascular risk (SURPASS-4): a randomised, open-label, parallel-group, multicentre, phase 3 trial, Lancet 398 (10313) (2021) 1811–1824, https://doi.org/10.1016/s0140-6736(21)02188-7.
[37] J. Rosenstock, J.P. Frías, H.W. Rodbard, S. Tofé, E. Sears, R. Huh, et al., Tirzepatide vs Insulin Lispro Added to Basal Insulin in Type 2 Diabetes: The SURPASS-6 Randomized Clinical Trial, Jama 330 (17) (2023) 1631–1640, https://doi.org/10.1001/jama.2023.20294.
[38] R. Patel, E. Kokori, G. Olatunji, F.A. Adejumo, J.D. Ukah, A.E. Babalola, et al., Therapeutic Potential of GLP-1 Receptor Agonists in Heart Failure with Preserved Ejection Fraction (HFpEF) in Obese Patients, Curr. Heart Fail. Rep. 22 (1) (2025) 17, https://doi.org/10.1007/s11897-025-00704-1.
[39] M. Chen, N. Zhao, W. Shi, Y. Xing, S. Liu, X. Meng, et al., Glucose-dependent insulinotropic polypeptide/glucagon-like peptide 1 receptor agonist tirzepatide promotes branched chain amino acid catabolism to prevent myocardial infarction in non-diabetic mice, Cardiovasc. Res. 121 (3) (2025) 454–467, https://doi.org/10.1093/cvr/cvaf005.
[40] M. Packer, M.R. Zile, C.M. Kramer, S.J. Baum, S.E. Litwin, V. Menon, et al., Tirzepatide for Heart Failure with Preserved Ejection Fraction and Obesity, N. Engl. J. Med. 392 (5) (2025) 427–437, https://doi.org/10.1056/NEJMoa2410027.
[41] C.M. Kramer, B.A. Borlaug, M.R. Zile, D. Ruff, J.M. DiMaria, V. Menon, et al., Tirzepatide Reduces LV Mass and Paracardiac Adipose Tissue in Obesity-Related Heart Failure: SUMMIT CMR Substudy, J. Am. Coll. Cardiol. 85 (7) (2025) 699–706, https://doi.org/10.1016/j.jacc.2024.11.001.
[42] Z.I. Hegedűs, M.E. Jakab, T.G. Gergely, N.V. Sayour, A. Kovács, S. Antal, et al., Tirzepatide, a dual GIP/GLP1-receptor co-agonist preserves cardiac function and improves survival in angiotensin II-induced heart failure model in mice: comparison to liraglutide, Cardiovasc. Diabetol. 24 (1) (2025) 253, https://doi.org/10.1186/s12933-025-02806-5.
[43] H. Ma, X.F. Dong, X.R. Cao, N.H. Hei, J.L. Li, Y.L. Wang, et al., Pro-Renin Receptor Overexpression Promotes Angiotensin II-Induced Abdominal Aortic Aneurysm Formation in Apolipoprotein E-Knockout Mice, Hum. Gene Ther. 31 (11-12) (2020) 639–650, https://doi.org/10.1089/hum.2019.124.
[44] A. Collado, P. Marques, P. Escudero, C. Rius, E. Domingo, S. Martinez-Hervás, et al., Functional role of endothelial CXCL16/CXCR6-platelet-leucocyte axis in angiotensin II-associated metabolic disorders, Cardiovasc. Res. 114 (13) (2018) 1764–1775, https://doi.org/10.1093/cvr/cvy135.
[45] Y. Nogi, M. Nagashima, M. Terasaki, K. Nohtomi, T. Watanabe, T. Hirano, Glucose-dependent insulinotropic polypeptide prevents the progression of macrophage-driven atherosclerosis in diabetic apolipoprotein E-null mice, PLoS. One 7 (4) (2012) e35683, https://doi.org/10.1371/journal.pone.0035683.
[46] M. Terasaki, H. Yashima, Y. Mori, T. Saito, Y. Shiraga, R. Kawakami, et al., Glucose-Dependent Insulinotropic Polypeptide Suppresses Foam Cell Formation of Macrophages through Inhibition of the Cyclin-Dependent Kinase 5-CD36 Pathway, Biomedicines 9 (7) (2021) 832, https://doi.org/10.3390/biomedicines9070832.
[47] R. Ortega, A. Collado, F. Selles, H. Gonzalez-Navarro, M.J. Sanz, J.T. Real, et al., SGLT-2 (Sodium-Glucose Cotransporter 2) Inhibition Reduces Ang II (Angiotensin II)-Induced Dissecting Abdominal Aortic Aneurysm in ApoE (Apolipoprotein E) Knockout Mice, Arterioscler. Thromb. Vasc. Biol. 39 (8) (2019) 1614–1628, https://doi.org/10.1161/atvbaha.119.312659.
[48] A.L. Golledge, P. Walker, P.E. Norman, J. Golledge, A systematic review of studies examining inflammation associated cytokines in human abdominal aortic aneurysm samples, Dis. Markers 26 (4) (2009) 181–188, https://doi.org/10.3233/dma-2009-0629.
[49] R.K. Middleton, G.M. Lloyd, M.J. Bown, N.J. Cooper, N.J. London, R.D. Sayers, The pro-inflammatory and chemotactic cytokine microenvironment of the abdominal aortic aneurysm wall: a protein array study, J. Vasc. Surg. 45 (3) (2007) 574–580, https://doi.org/10.1016/j.jvs.2006.11.020.
[50] H. Ahn, D.C. Kaelber, N. Hoell, R. Ambani, J.G. Quatromoni, A. Khalifeh, et al., Glucagon-like peptide-1 receptor agonists are associated with reduced abdominal aortic aneurysm-related events, e2, J. Vasc. Surg. 83 (4) (2026) 1079–1088, https://doi.org/10.1016/j.jvs.2025.11.021.
[51] M. Koshibu, Y. Mori, T. Saito, H. Kushima, M. Hiromura, M. Terasaki, et al., Antiatherogenic effects of liraglutide in hyperglycemic apolipoprotein E-null mice via AMP-activated protein kinase-independent mechanisms, Am. J. Physiol. Endocrinol. Metab. 316 (5) (2019) E895–e907, https://doi.org/10.1152/ajpendo.00511.2018.
[52] M. Punjabi, A. Kosareva, L. Xu, A. Ochoa-Espinosa, S. Decembrini, G. Hofmann, et al., Liraglutide Lowers Endothelial Vascular Cell Adhesion Molecule-1 in Murine Atherosclerosis Independent of Glucose Levels, JACC Basic. Transl. Sci. 8 (2) (2023) 189–200, https://doi.org/10.1016/j.jacbts.2022.08.002.
[53] G. Yang, Y. Lei, A. Inoue, L. Piao, L. Hu, H. Jiang, et al., Exenatide mitigated diet-induced vascular aging and atherosclerotic plaque growth in ApoE-deficient mice under chronic stress, Atherosclerosis 264 (2017) 1–10, https://doi.org/10.1016/j.atherosclerosis.2017.07.014.
[54] G. Rakipovski, B. Rolin, J. Nøhr, I. Klewe, K.S. Frederiksen, R. Augustin, et al., The GLP-1 Analogs Liraglutide and Semaglutide Reduce Atherosclerosis in ApoE(-/-) and LDLr(-/-) Mice by a Mechanism That Includes Inflammatory Pathways, JACC Basic. Transl. Sci. 3 (6) (2018) 844–857, https://doi.org/10.1016/j.jacbts.2018.09.004.
[55] M. Nagashima, T. Watanabe, M. Terasaki, M. Tomoyasu, K. Nohtomi, J. Kim-Kaneyama, et al., Native incretins prevent the development of atherosclerotic lesions in apolipoprotein E knockout mice, Diabetologia 54 (10) (2011) 2649–2659, https://doi.org/10.1007/s00125-011-2241-2.
[56] F. Kahles, A. Liberman, C. Halim, M. Rau, J. Möllmann, R.W. Mertens, et al., The incretin hormone GIP is upregulated in patients with atherosclerosis and stabilizes plaques in ApoE(-/-) mice by blocking monocyte/macrophage activation, Mol. Metab. 14 (2018) 150–157, https://doi.org/10.1016/j.molmet.2018.05.014.
[57] J. Helmstädter, K. Frenis, K. Filippou, A. Grill, M. Dib, S. Kalinovic, et al., Endothelial GLP-1 (Glucagon-Like Peptide-1) Receptor Mediates Cardiovascular Protection by Liraglutide In Mice With Experimental Arterial Hypertension, Arterioscler. Thromb. Vasc. Biol. 40 (1) (2020) 145–158, https://doi.org/10.1161/atv.0000615456.97862.30.
[58] A.E. Malavazos, G. Iacobellis, E. Dozio, S. Basilico, A. Di Vincenzo, C. Dubini, et al., Human epicardial adipose tissue expresses glucose-dependent insulinotropic polypeptide, glucagon, and glucagon-like peptide-1 receptors as potential targets of pleiotropic therapies, Eur. J. Prev. Cardiol. 30 (8) (2023) 680–693, https://doi.org/10.1093/eurjpc/zwad050.
[59] I. Hadjiyanni, K.A. Siminovitch, J.S. Danska, D.J. Drucker, Glucagon-like peptide-1 receptor signalling selectively regulates murine lymphocyte proliferation and maintenance of peripheral regulatory T cells, Diabetologia 53 (4) (2010) 730–740, https://doi.org/10.1007/s00125-009-1643-x.
[60] Y. Tashiro, K. Sato, T. Watanabe, K. Nohtomi, M. Terasaki, M. Nagashima, et al., A glucagon-like peptide-1 analog liraglutide suppresses macrophage foam cell formation and atherosclerosis, Peptides 54 (2014) 19–26, https://doi.org/10.1016/j.peptides.2013.12.015.
[61] L.M. Berglund, V. Lyssenko, C. Ladenvall, O. Kotova, A. Edsfeldt, K. Pilgaard, et al., Glucose-Dependent Insulinotropic Polypeptide Stimulates Osteopontin Expression in the Vasculature via Endothelin-1 and CREB, Diabetes 65 (1) (2016) 239–254, https://doi.org/10.2337/db15-0122.
[62] B.A. McLean, C.K. Wong, K.D. Kaur, R.J. Seeley, D.J. Drucker, Differential importance of endothelial and hematopoietic cell GLP-1Rs for cardiometabolic versus hepatic actions of semaglutide, JCI Insight 6 (22) (2021) e153732, https://doi.org/10.1172/jci.insight.153732.
[63] I.I. Shaikh, S. Singh, Y. Feng, K.A. Shahzad, J. Wang, Q. Zhou, et al., Therapeutic Targeting of Signaling Pathways in Abdominal Aortic Aneurysm: From

Pathogenesis to Precision Medicine, Drug. Des. Devel Ther. 19 (2025) 12077–12111, https://doi.org/10.2147/dddt.S563581.
[64] B.A. Borlaug, M.R. Zile, C.M. Kramer, S.J. Baum, K. Hurt, S.E. Litwin, et al., Effects of tirzepatide on circulatory overload and end-organ damage in heart failure with preserved ejection fraction and obesity: a secondary analysis of the SUMMIT trial, Nat. Med. 31 (2) (2025) 544–551, https://doi.org/10.1038/s41591-024-03374-z.
[65] L. Chen, X. Chen, B. Ruan, H. Yang, Y. Yu, Tirzepatide protects against doxorubicin-induced cardiotoxicity by inhibiting oxidative stress and inflammation via PI3K/Akt signaling, Peptides 178 (2024) 171245, https://doi.org/10.1016/j.peptides.2024.171245.
[66] X. Zhao, Z. Cheng, H. Zhang, Y. Guo, L. Zhao, C. Zhang, et al., Glucagon-Like Peptide-1 Inhibits the Progression of Abdominal Aortic Aneurysm in Mice: The Earlier, the Better, Cardiovasc. Drugs Ther. 38 (5) (2024) 873–884, https://doi.org/10.1007/s10557-023-07456-x.
[67] M.M. Thompson, L. Jones, A. Nasim, R.D. Sayers, P.R. Bell, Angiogenesis in abdominal aortic aneurysms, Eur. J. Vasc. Endovasc. Surg. 11 (4) (1996) 464–469, https://doi.org/10.1016/s1078-5884(96)80183-3.
[68] M. Kobayashi, J. Matsubara, M. Matsushita, N. Nishikimi, T. Sakurai, Y. Nimura, Expression of angiogenesis and angiogenic factors in human aortic vascular disease, J. Surg. Res. 106 (2) (2002) 239–245, https://doi.org/10.1006/jsre.2002.6468.
[69] I. Lingvay, O. Mosenzon, K. Brown, X. Cui, C. O'Neill, L. Fernández Landó, et al., Systolic blood pressure reduction with tirzepatide in patients with type 2 diabetes: insights from SURPASS clinical program, Cardiovasc. Diabetol. 22 (1) (2023) 66, https://doi.org/10.1186/s12933-023-01797-5.
[70] L.A. Cassis, M. Gupte, S. Thayer, X. Zhang, R. Charnigo, D.A. Howatt, et al., ANG II infusion promotes abdominal aortic aneurysms independent of increased blood pressure in hypercholesterolemic mice, Am. J. Physiol. Heart Circ. Physiol. 296 (5) (2009) H1660–H1665, https://doi.org/10.1152/ajpheart.00028.2009.
[71] Z. Zheng, Y. Zong, Y. Ma, Y. Tian, Y. Pang, C. Zhang, et al., Glucagon-like peptide-1 receptor: mechanisms and advances in therapy, Signal. Transduct. Target. Ther. 9 (1) (2024) 234, https://doi.org/10.1038/s41392-024-01931-z.
[72] C.K. Wong, D.J. Drucker, Antiinflammatory actions of glucagon-like peptide-1-based therapies beyond metabolic benefits, J. Clin. Invest. 135 (21) (2025) e194751, https://doi.org/10.1172/jci194751.
[73] Y. Dai, J.L. Mehta, M. Chen, Glucagon-like peptide-1 receptor agonist liraglutide inhibits endothelin-1 in endothelial cell by repressing nuclear factor-kappa B activation, Cardiovasc. Drugs Ther. 27 (5) (2013) 371–380, https://doi.org/10.1007/s10557-013-6463-z.
[74] K.K. Hannawa, J.L. Eliason, G.R. Upchurch Jr., Gender differences in abdominal aortic aneurysms (Suppl 1), Vascular 17 (1) (2009) S30–S39, https://doi.org/10.2310/6670.2008.00092.
[75] G. Ailawadi, J.L. Eliason, K.J. Roelofs, I. Sinha, K.K. Hannawa, E.P. Kaldjian, et al., Gender differences in experimental aortic aneurysm formation, Arterioscler. Thromb. Vasc. Biol. 24 (11) (2004) 2116–2122, https://doi.org/10.1161/01.Atv.0000143386.26399.84.
[76] M.W. Manning, L.A. Cassi, J. Huang, S.J. Szilvassy, A. Daugherty, Abdominal aortic aneurysms: fresh insights from a novel animal model of the disease, Vasc. Med. 7 (1) (2002) 45–54, https://doi.org/10.1191/1358863x02vm413ra.